Monitoring Lava Flows

Magdalena Oryaëlle Chevrel, Andrew J.L. J.L. Harris

Monitoring Lava Flows

Oryaëlle Chevrel[a,b,c] and Andrew Harris[a]

[a]*Université Clermont Auvergne, CNRS, IRD, OPGC, Laboratoire Magmas et Volcans, 63000 Clermont-Ferrand, France.*

[b] *Observatoire Volcanologique du Piton de la Fournaise, Institut de physique du globe de Paris, 97418, La Plaine des Cafres, France*

[c] *Université Paris Cité, Institut de physique du globe de Paris, CNRS, F-75005 Paris, France*

Table of content

Abstract 3
1. Introduction 3
1.1. Preamble 3
1.2. Type of lava flows and associated hazard 4
1.2.1. Lava flow types 4
1.2.2. Associated hazard and risks 5
1.3. Spatial coverage, time scales and definitions 6
1.3.1. Spatial coverage, time scales 6
1.3.2. Definition of source terms 7
2. Parameters to be measured 9
2.1. Mapping spatial extent and dimensions 9
2.2. Lava temperature (core and surface) 12
2.2.1. Thermocouples (core temperature) 12
2.2.2. A first idea of the surface temperature 14
2.2.3. Thermal infrared thermometer (surface temperature) 14
2.2.4. Thermal camera (surface temperature) 17
2.2.5. A short note on temperature retrievals from satellite-based sensors. 20
2.3. Lava surface velocity 21
2.4. Sampling 21
2.5. Lava flow morphology / typology 23
3. First Order derivatives 25
3.1. Building DEMs and volume estimation 25
3.2. Velocity profile and spreading rate 26
3.2.1. Velocity profile 26
3.2.2. Spreading rate 28

3.3. Heat Loss and Cooling rate 29
3.4. Sample chemical composition and texture 30
4. Second order derivatives 31
4.1. Volumetric discharge rate (volume flux) 31
4.1.1. Instantaneous effusion rate from lava velocity 31
4.1.2. TADR from volume, heat budget and flow area 32
4.1.3. Conversion to length 33
4.2. Rheological properties 33
4.2.1. Rheology from lava sample characteristics 33
4.2.2. Rheology of a lava flow 34
5. Hazard product: Lava flow modelling 35
6. Lava flow monitoring: The future 37
7. References 39

Abstract

During a volcanic effusive crisis, the active lava flow(s) need(s) to be monitored to best anticipate the possible affected area. A number of measurements needs to be made on site either from ground or from the air and by satellite imagery. These measurements need to be made through established protocols so derivative parameters can be calculated and extracted to contribute to forecasting and reduce possible impacts of lava flows. Measurements and reporting parameters include lava flow setting, morphological description, dimensions (thickness, length, width, underlying slope), temperature (core and surface), and sampling. First order derivative are topographical changes, estimation of emitted lava volume, lava flow velocity (channel and front), cooling rate, petrology and lava flow type characteristics. Second order derivative then involve volumetric discharge rate estimation, heat budget models and rheological constrains. These are essential parameters that are part of the monitoring duties and feed lava flow hazard projection and numerical modelling. In this chapter, we review the measurements that are typically made and the subsequent derivatives that all contribute to monitoring activities during an effusive event.

1. Introduction

1.1. Preamble

As a member of an agency, such as a volcano observatory, charged with monitoring and surveillance during an effusive crisis you will have to focus on making observations and measurements necessary to meet the reporting requirements of the agency. There is a lot to do, and you will usually be understaffed and overworked. Worse, the lava flow may be in a remote area, you will unlikely have helicopter support and will have to walk many kilometers over difficult terrain carrying all that you need. To reach the lava, unlike when monitoring air fall or a geophysical signal, you have to go to it and directly approach the source so as to collect samples or measure the interior temperature. On return to the office you will need to work up and process the data you have collected, enter them into a data base, use them for numerical modelling and prepare a written or oral report. These can be daily, weekly and/or monthly for both internal and external use, as well as press-release, depending on the eruption location, threat and duration.

There will be a protocol in place for the measurements that need to be made as well as the format and content of reporting duties. Thus, all you have time to carry out are the routine measurements as there may be no time to set up experiments for scientific research paper. In

this chapter, we review the measurements that are typically made to contribute to monitoring activities during an effusive event. These fall into three linked categories which will provide information for reporting. They are (**Fig. 1**):

1. The measurements that need to be made in the field;
2. First order derivatives which are made from data collected in the field or via remote sensing; and
3. Second order derivatives that use the first order product to carry out calculations.

A fourth level of modelling can contribute to forecasting and will feed back into the reporting (**Fig. 1**). The objective of the chapter is to describe how to carry out these measurements, calculations and modelling.

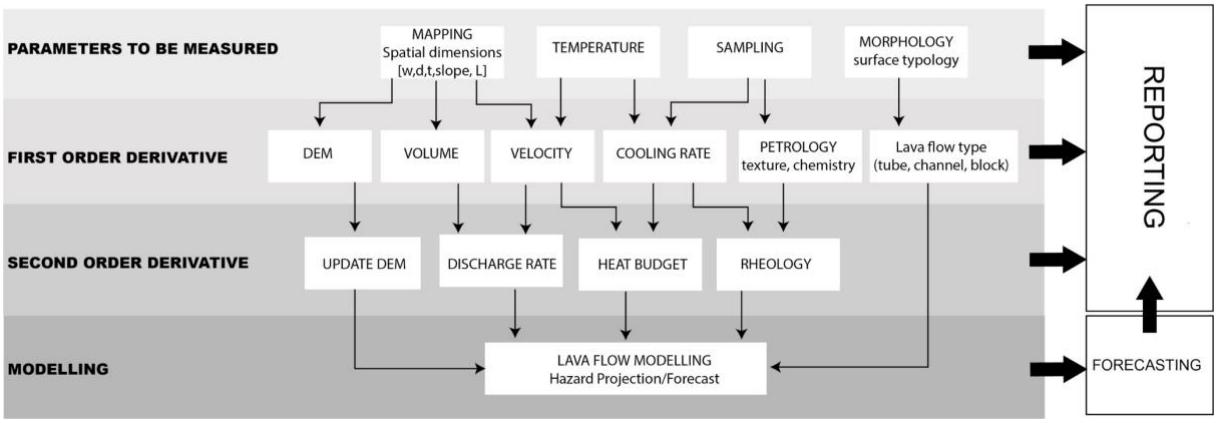

Figure 1: Flow chart tracking the series of measurements and calculation of derived parameters that are typically made to contribute to monitoring activities during an effusive event.

1.2. Type of lava flows and associated hazard

1.2.1. Lava flow types

Lava flows are gravity currents propagating downslope under their own weight, slowed by their own viscosity and core or crust yield strength, which increase with cooling and crystallization. Their velocity, morphology, shape, width and length mainly depend on the effusion rate (i.e., lava volume flux leaving the vent), the total volume emitted, topography and the thermo-rheological properties of the lava. Typically, the higher the rate of effusion and the volume, the longer the flow, and the lower the viscosity and the steeper the slope, the faster the flow. Advance stops when the supply of lava stops (volume-limited flow) or when cooling is such that the flow viscosity reaches a limit that prevents further motion (cooling-limited flow).

The different types of lava flows are distinguished according to their composition, their morphology and their dynamics. Silica-poor lava flows (e.g., basaltic flows) are the hottest and

most fluid and can reach speeds of several km/h. Flow types are generally pāhoehoe, with a smooth, coherent surface, and ʻaʻā with a surface comprising a layer of clinker. Flows can be channel or tube-fed, and can extend from a few to a few tens of kilometers. The formation of tubes insulates the lava, reducing cooling rates and allowing the lava to extend greater distances, where the longest lava tubes on Earth are more than 100 km long. More siliceous compositions (andesite, dacite and rhyolite) are colder, highly viscous and their advance rate does not exceed a few m/day. Their thickness is generally several tens of meters and their surface is often made of angular blocks which can reach sizes of the order of a meter. Silicic lava flows can, though, extend several kilometers, where flow front collapses can depressurize the flow interior to feed pyroclastic flows of the block-and-ash type.

1.2.2. Associated hazard and risks

Lava flows represent one of the most frequent volcanic hazards on a global scale, however, they rarely pose a safety risk to populations (Harris, 2015). Deadliest examples are those of the Nyiragongo eruptions in the Democratic Republic of Congo (DRC) in 1977, 2002 and 2021. These eruptions involved extremely fluid lava flows that moved to high velocities and reached the city of Goma, 10 km to the south of the source vents, in just a few hours. These eruptions each accounted for several tens of fatalities, from direct contact with lava, collapse of buildings, and explosion of fuel tanks.

Even if these human losses due to lava flows are minimal compared to those of other volcanic phenomena (they represent only 0.2% of the total deaths linked to volcanic hazards – (Harris, 2015)), they nonetheless destroy, burn and bury all infrastructure and vegetation in their path, having lasting effects on local economies. The 2018 effusive eruption of Kīlauea in Hawaii which lasted only 4 months (Neal et al. 2019) caused no casualties, but destroyed more than 700 houses and caused losses estimated at over $800 million (Meredith et al. 2022). The 2021-2022 eruption of La Palma (Canaries), buried ca. 1200 ha of land including agricultural land and villages, destroying more than 1600 houses and involved displacement of more than 7000 people (Cabildo de la Palma: https://riesgovolcanico-lapalma.hub.arcgis.com).

When the lava comes into contact with water, the instantaneous thermal expansion of the water causes littoral explosions, while persistent entry of lava into the ocean can build benches. Benches are unstable, and often collapse so that ocean entry sites are extremely dangerous for visitors. Vaporization of sea water at ocean entries also feeds persistent gas plumes named lazes. Lazes and gas plumes associated with emission of lava at the vent, that could create a volcanic smog (called vog), are loaded with fine particles, as well as harmful gases and aerosols

(HCl, CO_2, NO_2 and SO_2; (Hansell and Oppenheimer 2004). At source, they are also extremely hot so that inhalation of the gas can be fatal due to extreme lung damage. Wet and dry acid deposition can also damage infrastructure, through corrosion, as well as crops, forest and habitat (Blong 1984; Schmidt 2015).

Flow front collapses at silicic lava flows can represent a significant hazard due to the associated block and ash flow (Harris et al. 2002; Pallister et al. 2019). A flow front collapse at Santiaguito (Guatemala) in 1922 resulted in thousands of casualties (Rose 1987). Locations immediately down slope of an active silicic lava flow are thus extremely dangerous places to live and work.

1.3. Spatial coverage, time scales and definitions

1.3.1. Spatial coverage, time scales

Lava flow monitoring can be carried out from three locations: ground, air and space. Each vantage point allows differing spatial coverage and time scales of change to be tracked, increasing from local and rapid for the ground observer to synoptic and regular from satellites. Ground-based surveys include rapid, real-time measurements usually focusing around the key elements of the flow field: the vent, the channel or tube, and flow front. Ground-based surveys are usually carried out on foot, and have increasingly been supported by surveys by unmanned aerial systems or vehicles (UAS-UAV, see review from James et al., 2020). UAS surveys cover a few m^2 to hundreds of m^2 and are performed from heights of typically ≤120 m. This allows greater coverage, is faster than walking the edge of a flow unit, and allows access to zones that are impossible to approach on foot. However, like measurements made on foot, UAS surveys cover only a restricted time slot of a few minutes.

Airborne surveys are measurements performed from helicopter or any aircraft and cover area of few km^2 to 10's km^2. These operations are performed from higher altitudes, between 300 and 1500 m, than via UAS and may be ran over several hours.

From space, satellite acquisition includes geostationary as well as polar orbiting satellites allow synoptic coverage at wavebands spanning the ultraviolet, through the visible to the infrared and radar. However, only the latter is not affected by cloud cover.

Effective monitoring of lava flows combines observations from each of these three locations. Observations are complementary, and ideally data acquired from all three locations are combined to ensure a full coverage of the advancing lava flow. For example, while the ground-based observation can be used to ground truth a point satellite-sensor-derived image, the image can be used to extend knowledge beyond the isolated points visited on the ground.

1.3.2. Definition of source terms

A key source term for lava flow monitoring is the volumetric discharge rate (in m^3/s). This has three definitions depending on the temporal scale (**Fig. 2a**; see also Harris et al., 2007) over which the flux is measured:

1. *Instantaneous effusion rate (IER):* This is the volume flux measured at any single point in time. It is primarily measured in the field at the master channel or tube using the cross-sectional area (in m^2) of the flow multiplied by the flow velocity (in m/s).
2. *Time-averaged discharge rate (TADR)*: This is the volume flux averaged over some period of time. This is the value typically obtained from satellite infrared data or from DEM subtraction during the eruption. In this latter case, the volume of the lava flow field on day *n* is subtracted from the volume of day *n+i*. The residual volume is then divided by the time between the two measurements to give the time-averaged flux during the *i* days between the two volume measurements.
3. *Mean output rate (MOR)*: This is the total volume erupted during the entire eruption, or eruptive phase (usually obtained by DEM difference pre and post eruption), divided by the duration of the eruption.

As we move through these measurements, the discharge rate curve becomes increasingly smoothed and we lose the detail of peaks and troughs (**Fig. 2a**). The absolute value of the peak fluxes also becomes reduced, which is something to bear in mind when applying predictive models that relate volume flux to flow runout.

The flux measurement will also be influenced by where in the system the measurement is made (**Fig. 2b**). The *total* volume flux can only be measured at the master channel or tube exiting the vent and through which all of the volume passes. In a bifurcating system, after the first branch a *local* flux will be measured which will be less than the total flux as the volume is beginning to be partitioned between different distributaries. Finally, a *point* flux will be obtained at a flow front lobe when many lobes are active (**Fig. 2b**).

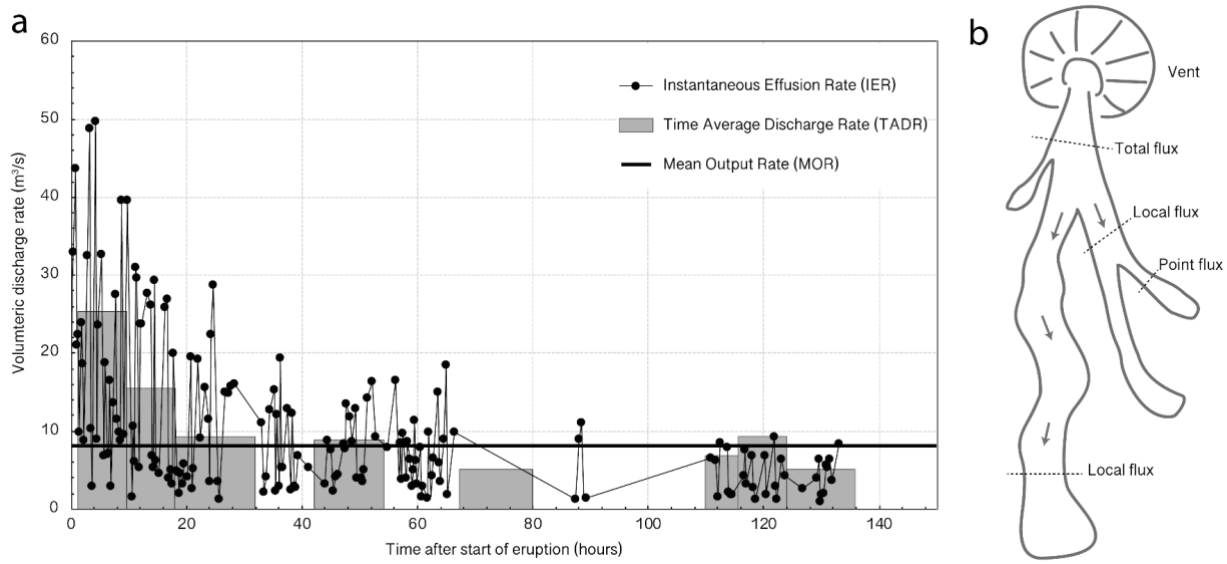

Figure 2: Discharge rate definition over a) time and b) in space.

We need also to distinguish between bulk and dense rock equivalent (DRE) volume fluxes. The bulk measurement includes all fluid and bubbles, as well as cracks in solid lava and spaces between clasts in an 'ā'a flow. In contrast, the DRE only consider the solid phase and does not include bubbles. This can be quite an issue as at the vent bubble contents can be very high and usually decreases toward flow front. Worse, bubble contents can vary with time during an eruption. Thus, volume flux measurements should always be taken, or reported, in tandem with a measure of the bubble content. As a result of all inherent sources of error, the uncertainty on a volume flux measurement is often at least 50 %. Thus, numbers (below) 100 should be reported to the nearest decimal place; above100 to the nearest round number; and above 500 to the nearest ten, etc.

Finally, the spatial position of flow velocity also needs to be well defined because it changes down system depending slope, flow depth and rheology. Fundamentally, channel velocities measured at any given point down system will be higher than the flow front advance rate, with the latter measurement being fundamental for hazard assessment. Velocity will also vary between the flow surface and base, and from bank to bank. Velocity across and within a channel may present a gradient from zero at the sides and base to a maximum at the channel center and surface. Thus, the spatial point at which the velocity measurement is made must be noted so that it can be related to the maximum and mean velocity (see later), both in terms of position across a channel, as well as down system.

2. Parameters to be measured

2.1. Mapping spatial extent and dimensions

Monitoring lava flows starts with acquiring the geographic coordinates of the eruption site. This requires location on the Global Navigation Satellite System (GNSS) for the ends of the eruptive fissures and thus also their length and strike, or point a location of single vent. Then, the flow front position is next most important point to locate, and hence the flow length at time *t*. The evolving length should then be tracked. Ideally flow outline and thickness should be obtained too, and terrain and topography updated so as to allow the trajectory of any new flow to be assessed. As the eruption goes on, repeat surveys ensure an effective monitoring.

Fissure or vent location can be obtained by hiking to the eruption site with handheld GNSS. However, lava flows often occur in remote places, and it is often difficult, or impossible to get close to the vent (in particular due to the ongoing eruption). In this case, airborne survey is the most efficient manner to get rapidly to the eruption site and acquire the required coordinates with a handheld GNSS. Since the 1980's, reconnaissance overflights have been mainly operated using helicopters. Satellite images are also consulted to detect the associate hotspot and may rapidly provide localization of the lava flow extent although at low resolution (1–4 km/pixel), or more precisely if there is an overpass by a satellite with higher (30-60 m/pixel) spatial resolution (see chapter Monitoring Heat). Final options for an approximate location of the eruptive vent are localization of the tremor sources and use of webcam networks.

During an eruption, the extent of an expanding flow can be tracked in multiple ways, depending on the flow setting and dimensions, and on observatory funds where some techniques are cheaper than others. Ground-based mapping can either be done by walking the flow limits with handheld differential GNSS, using webcam networks or by UAS. UAS-derived photographs can be stitched together to construct georeferenced orthomosaics from which the outline of the flow can be drawn. Additionally, these photographs can be used for photogrammetry applying structure from motion (SfM) technique to reconstruct the 3D topography and produce an updated DEM. Over the past decade, this technique has become common. As mentioned above, UAS-based survey is ideal for areas of less than 1 km^2, to map parts of the flow, local features, vent areas, breakouts and flow fronts. However, flow-field-wide orthomosaics and DEMs exceeding a few km squares need airborne surveys to be carried out by ultralight aircrafts or helicopters (**Fig. 3**).

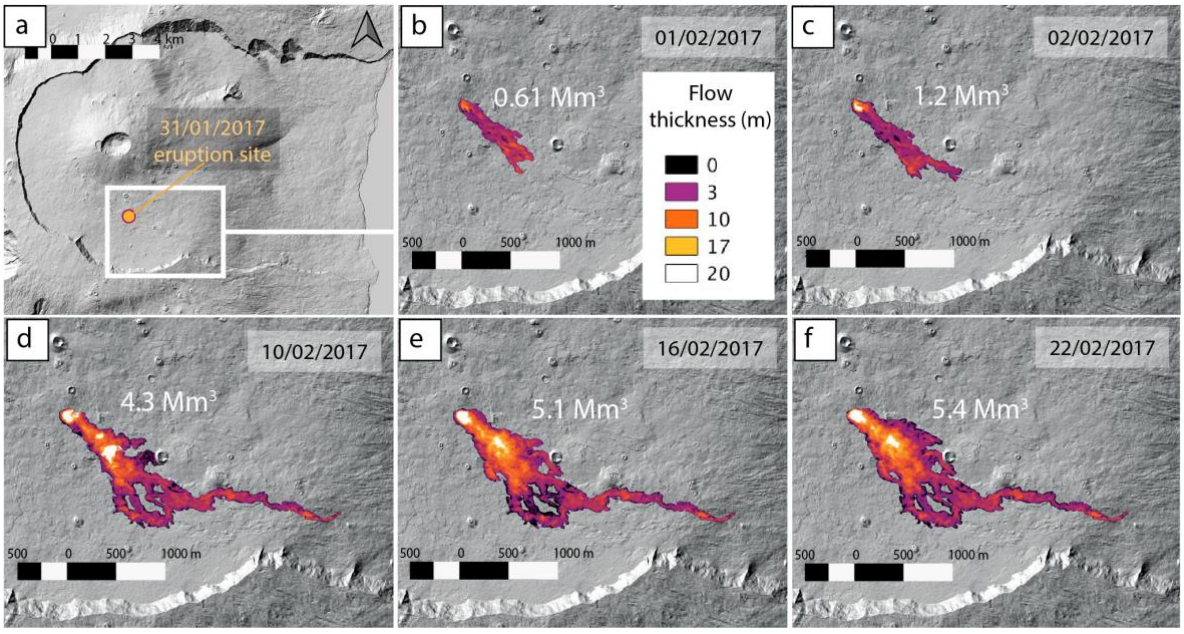

Figure 3: a) Location of the eruptive site of the 31 January – 27 February 2017 eruption of Piton de la Fournaise volcano, La Réunion. b-f) evolution of the flow area, thickness (in m) and corresponding volume (in Mm^3) has obtained from repeat photogrammetric campaigns. Figure modified from Derrien (2019).

Moving to the airborne perspective, in Hawaii, helicopter overflights were carried out every week, and sometimes daily, during the last recent effusive crises. Images acquired by a handheld thermal camera from an airborne survey were used for mapping (Patrick et al. 2017). Airborne Light Detection and Ranging (LiDAR) surveys can also be conducted to allow millimeter topographic precision, though coverage is usually local and costs are high. At Piton de la Fournaise (La Réunion), lava flow field evolution is usually mapped via ultralight aircraft surveys, which have a more reasonable price (**Fig. 3**).

Satellite imagery is the most efficient way to track the evolution of lava flow fields and to map entire lava flow fields with a single image. Satellite thermal and visible imagery (see chapter Monitoring Heat) have spatial resolutions of 30 m (TM, ETM+, ALI, ASTER) to a meter (Planet Labs) and to sub-meter (e.g., GeoEye and WorldView satellites). In case of cloud coverage that hinders thermal and visible imagery to be exploited, satellites equipped with radar sensors are used to monitor ground surface displacement through Interferometry Synthetic Aperture Radar (InSAR) (e.g., ERS, Envisat, TerraSAR-X, Sentinel 1, ALOS-2). InSAR allows the newly emplaced lava flow to be seen by comparing an image before and after lava flow emplacement because it results in a highly incoherent surface (low coherence, **Fig. 4**). Coherence maps can therefore be used to define the lava flow outline under any weather conditions (Bato et al. 2016; Dietterich et al. 2012; Harris et al. 2019; Poland 2022).

281

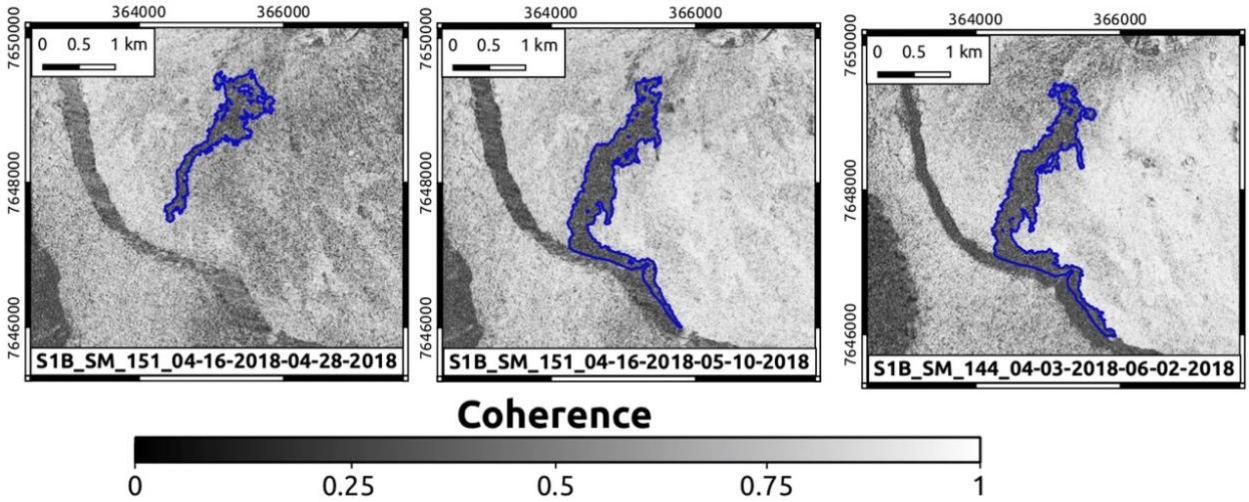

282 **Figure. 4.** Evolution of the flow outlines and extension of the lava flow field as mapped from
283 InSAR coherence maps obtained via the Oi^2 platform (https://opgc.uca.fr/volcanologie/oi2)
284 during the April 2018 eruption of Piton de la Fournaise (modified from Harris et al., 2019).

285

286 Recent advances in mapping from satellite imagery is the Copernicus Emergency Management
287 Service (Copernicus Emergency Management Service 2022; https://emergency.copernicus.eu/)
288 that since 2012 has provided geospatial information through a no-cost mapping service in cases
289 of natural disasters within hours or days from the activation of support via their emergency
290 management activities for a natural disaster, including volcanic eruptions. In 2021, the
291 Copernicus Emergency Management Service provided a first precise lava flow map just two
292 days after the May 2021 Nyiragongo (RDC) eruption. The service was also extremely effective
293 in mapping the flow expansion during the 2021 eruption of La Palma (Spain) (**Fig. 5**).

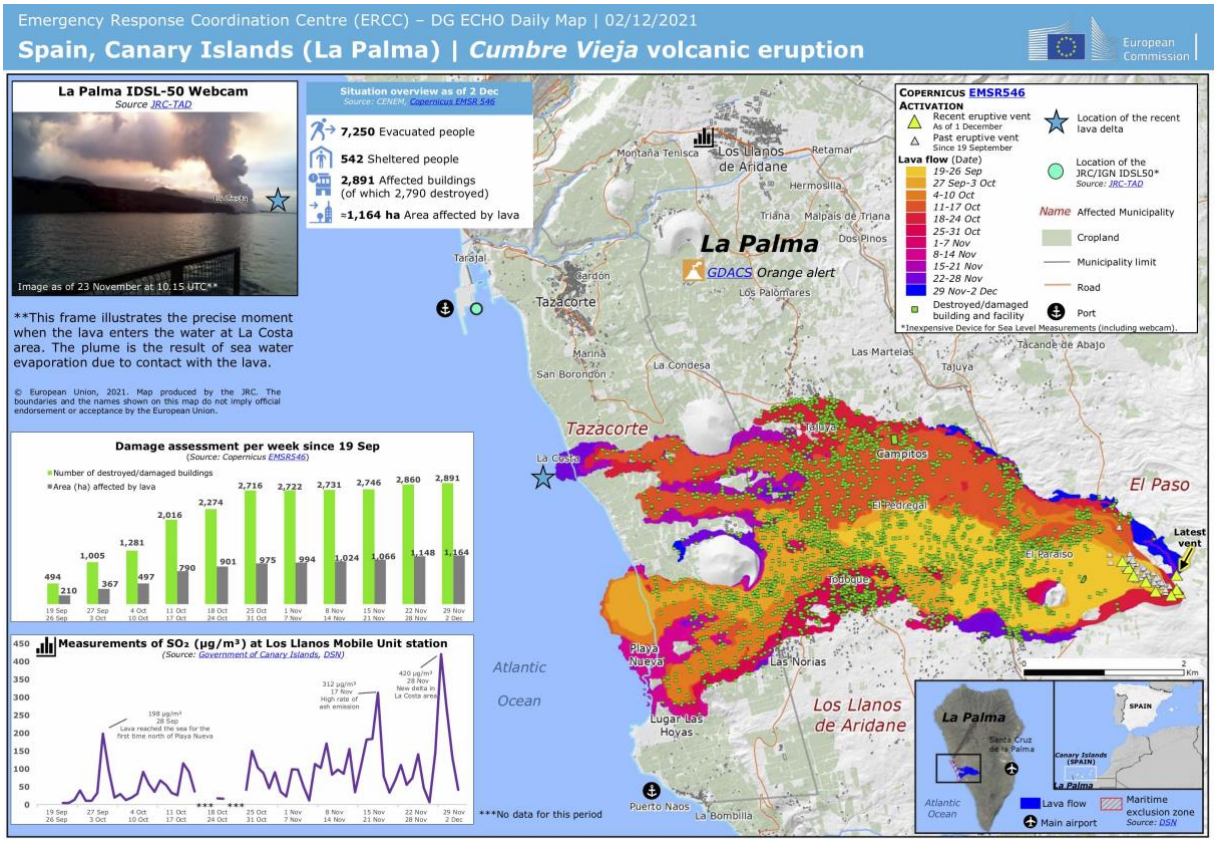

Figure 5: The Emergency Response Coordination Centre (ERCC) daily map for the La Palma (Spain) lava flow field for 2 December 2021. *Copernicus Emergency Management Service (© European Union, 2012-2022)*

2.2. Lava temperature

2.2.1. Thermocouples (core temperature)

The optical approach gives the surface temperature, so that a thermocouple is required to obtain the temperature of the flow interior. The interior temperature is typically hundreds of degrees centigrade hotter than the surface, and is the temperature we need to assess the eruption temperature, for down-flow cooling estimates and modelling. The thermocouple consists of two wires with a junction at the penetrating end, protected by a metal sheath and connected to a read out. The thermocouple is plunged into the lava and the temperature recorded. There are five concerns involved when making this measurement:

1. Probes are typically less than a meter long (e.g., **Fig. 6**). The measurement thus requires close approach to the active lava, which will have surface temperatures greater than 800 °C and interior up to more than 1100 °C. This can be at best uncomfortable and at worst painful, and means that all exposed flesh needs to be well covered to avoid radiation burns. Approach, if possible, should also be made up-wind, which is especially true at skylights where heated air blowing

out of the tube system can have temperatures >600 °C. A fire suit and helmet is one solution (**Fig. 6**), and metal shield can be used to stop the radiation from the lava. A longer probe could be another solution, but as they become longer than 1 m they tend to bend upon insertion, making penetration difficult. In that case, the probe can be attached to a rigid steel pole of 1 to 2 meters that would ease penetration into the lava flow although this adds to bulk and weight.

2. To protect the delicate wires, a metal sheath is used. To allow protection in the extreme environment of a lava flow, as well as during penetration, this needs to be at-least 3 mm thick. Such a thickness is also required to allow the probe to penetrate the surface crust without it bending thus failing to pass through the crust. However, the sheath needs time to heat up which means that the reading will pick up over a period of one to two minutes. Once the reading is stable the measurement is made. This means that the operator needs to stay in-situ for the same amount of time.
3. Due to lava quenching to the probe, the sensor may not heat to the same temperature as the surrounding probe. In such a case, the reading will begin to decline without stabilizing and the probe should be withdrawn. It is thus best to (i) have a pre-measurement idea of what the maximum temperature should be, and (ii) continue to make the measurements until you have at-least three that are the same and stable.
4. Care should be taken not to ground the probe on the cooler flow base, and to ensure that the probe is well within the fluid interior and not in the cooler visco-elastic crust. Finally, you should constantly stir to (i) avoid lava quenching to the probe, and (ii) avoid the probe becoming entrapped in the constantly forming surface crust.
5. If the flow is too large, close approach will not be possible due to the radiative heat and/or the measurable zones maybe inaccessible in a sea of hot, recently emplaced lava. Also, flow margins may be too unstable to allow safe approach and/or flow surface in a channel may be too far below the levee rim. The easiest targets to measure are small pāhoehoe lobes (**Fig. 6a**), or slowly moving breakout through lava front or margin (**Fig. 6b)** but these are not always available or accessible.

Remember, that upon completion of the measurement the metal sheath of the thermocouple will remain extremely hot for several minutes, so on no account touch it. Also, after each

measurement, the lava attached to the probe will need to be quenched into water, so it will break off, or need to be knocked off with a hammer.

Figure 6: Measuring lava temperature with K-type thermocouple that is 60 cm long and 3 mm thick sheath and linked to a data logger at a) pāhoehoe lava lobe (Hawaii, 2016; photo: © USGS, M. Patrick) and b) at an 'ā'a flow front (Piton de la Fournaise, La Reunion, 2019) (photo: © L. Perrier).

2.2.2. A first idea of the surface temperature

The simplest way to have a ball-park estimation of lava surface temperature was visually by matching surface color to the temperature associated with that color. This best done at night and is the principle of the optical pyrometer. The pyrometer consists of a heated wire, the temperature of which is adjusted to change the color at which it glows. When viewed against active lava, the point at which the color of the wire is not distinguishable from the surface in the background gives the temperature of that background. Alternatively, the assessment can be made visually and a lookup table used to assess the temperature (Harris, 2013).

2.2.3. Thermal infrared thermometer (surface temperature)

The thermal infrared thermometer uses radiated heat to obtain surface temperature and usually work with spectral radiant exitance in the 8–14 μm range. Note that, given the high temperature range of active lava surfaces, a model which can measure the full range of expected temperatures from ambient out to 1200 °C needs to be used. Being a remotely sensed measurement, no close approach is necessary. However, the measurement is of a radiative temperature (T_{rad}) and will not be the kinetic temperature. That is, most bodies are not perfectly emitting blackbodies, so that spectral radiant exitance from a surface emitting at kinetic temperature T_{kin} and wavelength λ will be reduced by a factor described by the emissivity (ε). Spectral radiant exitance, $M(\lambda,T)$, varies as a function of wavelength and temperature (T), and is given by the Planck function:

$$M(\lambda,T) = c_1\lambda^{-5}\left[exp^{\frac{c_2}{\lambda T}} - 1\right]^{-1} \quad (1)$$

Here c_1 and c_2 are constants with the values of 3.741×10^{-16} W m^2 and 1.4393×10^{-2} m K, respectively. Note that units of wavelength and temperature thus need to be in units of meters and Kelvin, and M(λ,T) has the units W m^{-2}, i.e., J s^{-1} m^{-2}.

Equation (1) applies to a black body, however for a body with an emissivity less than one the function becomes:

$$M(\lambda,T_{rad}) = \varepsilon\, M(\lambda,T_{kin}) = \varepsilon\, c_1\lambda^{-5}\left[exp^{\frac{c_2}{\lambda T}} - 1\right]^{-1} \quad (2)$$

Thus, to obtain the actual surface temperature, we need to convert the radiative temperature to a spectral exitance using Equation (1), divide the value of M(λ,T) by emissivity, and convert the result back to temperature, which will now be a kinetic temperature. This can be done by inverting the Planck function:

$$T_{kin} = \frac{c_2}{\lambda \ln\left(\frac{\varepsilon\, c_1\, \lambda^{-5}}{M(\lambda,T_{rad})} + 1\right)} \quad (3)$$

Emissivity will vary with wavelength and surface type, where those for typical lava surface types are given in **Table 1**. There is debate over what the emissivity for a molten surface should be and evidences that emissivity changes with temperature and composition (Biren et al. 2022; Burgi et al. 2002), but the values of **Table 1** are those typically used.

Location	Type	Emissivity 8 – 14 μm
Kilauea	Basalt: pāhoehoe	0.901
Kilauea	Basalt: ‘ā’a	0.954
Kilauea	Basalt: pāhoehoe – ropey	0.943
Kilauea	Basalt: pāhoehoe – smooth, glassy	0.900
Kilauea	Basalt: pāhoehoe – vesicular	0.909
Etna	Basalt: pāhoehoe – slabby (spiny)	0.957
Etna	Basalt: ‘ā’a	0.971

Table 1: Band-averaged emissivity values for a range of lava flow types (from Harris, 2013b). Note that these are values for cold sample, and not molten material.

It must be recalled that the measured surface temperature will likely not be that of the interior. Rapid radiative cooling, for example means that the surface temperature can cool by 50–300 °C within a second of exposure. On well-crusted, mature flows, the difference between the surface and interior temperature will be greater still (**Fig. 7**).

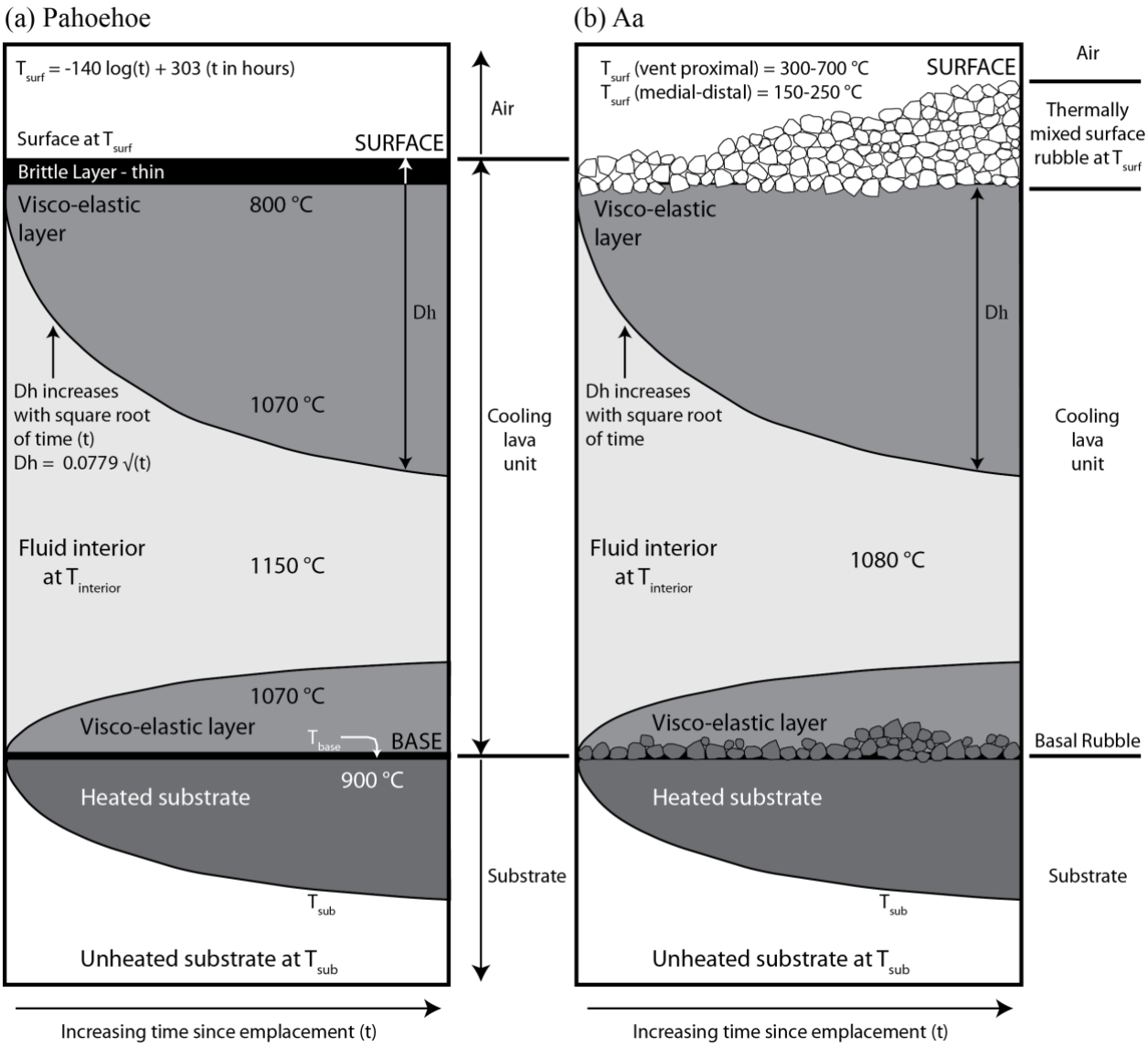

Figure 7: Thermal layers in (a) a pāhoehoe lobe and (b) an ‘ā’a flow and their evolution with time (after (Harris, 2013). For pāhoehoe, cooling and layer depth relations are from (Hon et al. 1994), as are the temperatures at the contact between each thermo-rheological layer and are for Hawaii. T_{base} is the basal contact temperature and is from (Keszthelyi 1995). For ‘ā’a surface temperatures for the proximal and medial-distal are for ‘ā’a channels at Piton de la Fournaise, La Réunion (Harris et al., 2019) and Lonquimay, Chile (Oppenheimer 1991), respectively; and interior temperature is for ‘ā’a erupted during Etna (Itlay) 1991–1993 eruptions (Calvari et al. 1994). As apparent, while the thermocouple temperature must be made for the interior, and measurement can only be made when the crust is thin and immature, the surface temperature will not reflect the interior temperature. However, the surface temperature is what we need in order to estimate heat fluxes and cooling rates.

409

410 ### 2.2.4. Thermal camera (surface temperature)

411 Thermal cameras tend to operate in the same waveband as thermal infrared
412 thermometers (7.5–14 μm), but provide temperatures for an array of pixels providing a thermal
413 image rather than a single spot temperature. Focal plane arrays tend to comprise 640 × 480
414 pixels, with each pixel having an instantaneous field of view (IFOV) of 0.65 mrad and the image
415 having a standard total field of view (TFOV) of 24 × 18 ° (or 45 × 12 ° wide lens are also used).
416 For a perfectly horizontal or vertical field of view the pixel or image diameter field of view
417 (D_{FOV}) can be calculated using the simple trigonometric relation:

418 $$D_{FOV} = 2\,[D \tan(\beta/2)] \quad (4)$$

419 Where D is the distance to the pixel or image center and β is the angular IFOV or TFOV. If the
420 ground within the field of view is sloping, then D_{FOV} should be corrected for slope (α):

421 $$D_{FOV}\ (\text{slope corrected}) = D_{FOV} / \cos(\alpha) \quad (5)$$

422 For oblique viewing angles calculating the field of view dimensions requires the viewing angle
423 (θ) to be taken into account (**Fig. 8**). For a viewing position *h* meters above the surface, this can
424 be done using:

425 $$D_{FOV} = h\left[tan\left(\theta + \frac{\beta}{2}\right) - tan\left(\theta - \frac{\beta}{2}\right)\right] \quad (6)$$

426 For a viewing position *x* meters away from the surface (**Fig. 8**), calculation of D_{FOV} requires
427 replacing *h* with *x* in Equation (6).

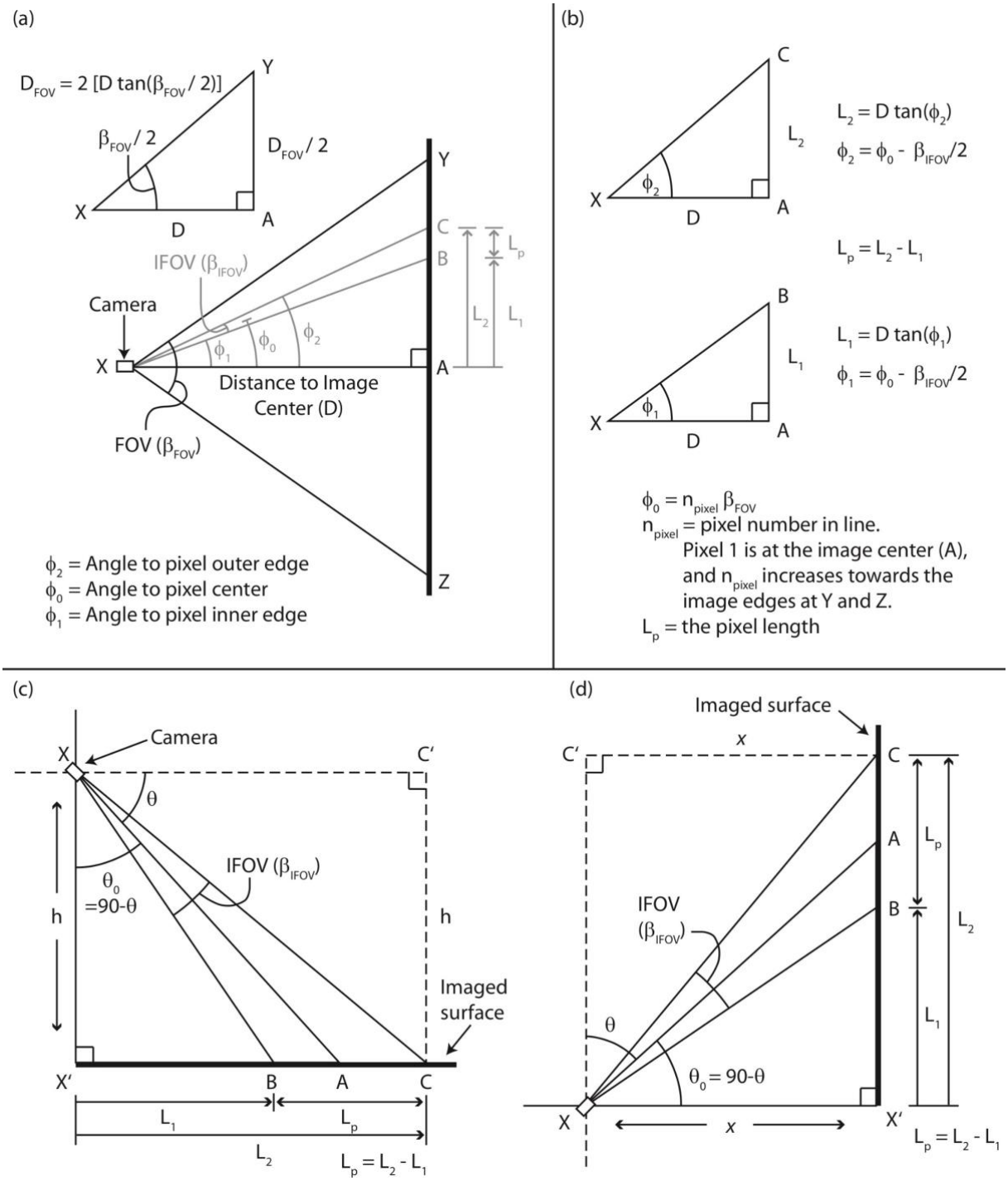

Figure 8: (a) Geometry for calculating pixel and image size for a flat surface viewed at right angles, with triangle required to calculate the total image field of view (FOV). Geometry for calculating the size of pixels within this FOV is in gray. (b) Triangles required to calculate the pixel size (L_{pixel}) using the detector instantaneous field of view (IFOV). (c) Geometry for calculating pixel size for a surface imaged by looking downwards, and (b) looking upwards. Modified from (Harris, 2013).

Pixel temperatures will be subject to the same emissivity correction as described for the thermal infrared camera, but also (for distances greater than 100 m) requires atmospheric correction. The signal received by the camera will be a mixture of the surface emitted radiant

exitance, $\varepsilon M(\lambda,T)$, as well as that emitted by the atmosphere, termed atmospheric upwelling radiance (M_U). This will all be modified by atmospheric absorption (ψ) as described by transmissivity ($\tau = 1 - \psi$). Thus, the temperature recorded by the camera is a brightness temperature (T*) given by (**Fig. 9**):

$$M(\lambda,T^*) = \tau(\lambda)\varepsilon(\lambda)M(\lambda,T_{kin}) + M_U(\lambda) \quad (7)$$

Atmospheric correction thus needs to take into account the emissive and absorptive properties of the atmosphere. This can be done by re-arranging Equation (7) so that,

$$M(\lambda,T_{kin}) = [M(\lambda,T^*) - M_U(\lambda)] / [\tau(\lambda)\varepsilon(\lambda)] \quad (8)$$

The atmospheric properties will vary with altitude and distance. The atmosphere becomes thinner with increased altitude and decreased path length, so that M_U and τ decrease accordingly. Typical correction values, as a function of altitude and distance are given in **Figure 9**.

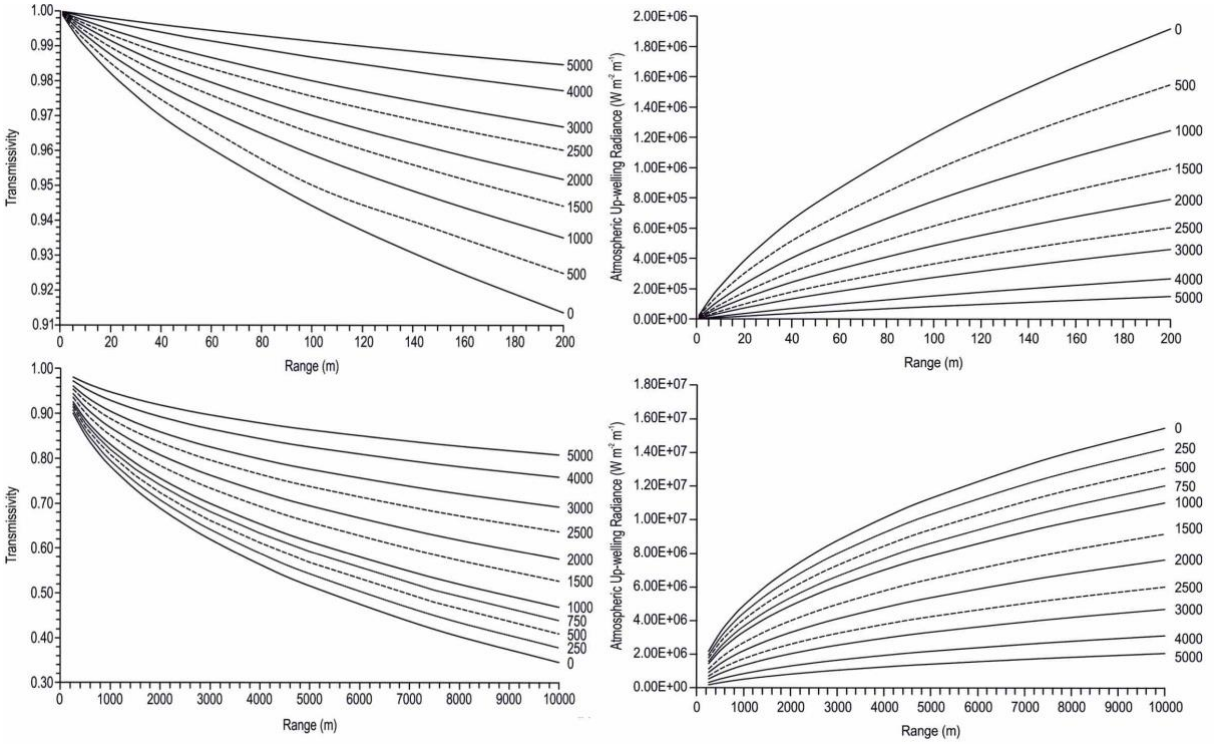

Figure 9: Increase in atmospheric transmissivity (left graphs) and upwelling radiance (right graphs) for a horizontal line of sight (LOS) at a range of altitudes between 0 to 10 000 m (top graphs is a zoom over 0 to 200 m). Values were obtained using MODTRAN with 1976 US Standard atmosphere and a CO_2 mixing ratio of 380 ppm·v across the 7.5 µm to 13 µm waveband and are plotted from Tables in (Harris, 2013). Note that, after a distance of only 10 m transmissivity begins to become an issue, with almost 6 % of the signal being absorbed by a distance of 100 m at sea-level. At ambient temperatures, upwelling radiance is an issue, accounting for 20 % of the signal received by an infrared detector placed at a distance of 1 km from a surface at 0 °C. However, for higher temperatures the contribution is not so important, being 3 % for surfaces at 200 °C and 1 % for surfaces at 500 °C

(see Harris, 2013). Thus, at higher temperatures the correction for upwelling could be ignored for an approximation of kinetic temperature, but transmissivity cannot.

The thermal camera measurement principles are the same whether the camera measurement is made from the ground or an aircraft. For airborne measurements the craft needs to fly sufficiently slowly so as to avoid image smearing, and doors must be off otherwise the temperature of the glass, which is 100 % opaque in the infrared, will be recorded. However, for both cases to solve the relations given above the acquisition conditions need to be recorded, as given in **Figure 10**.

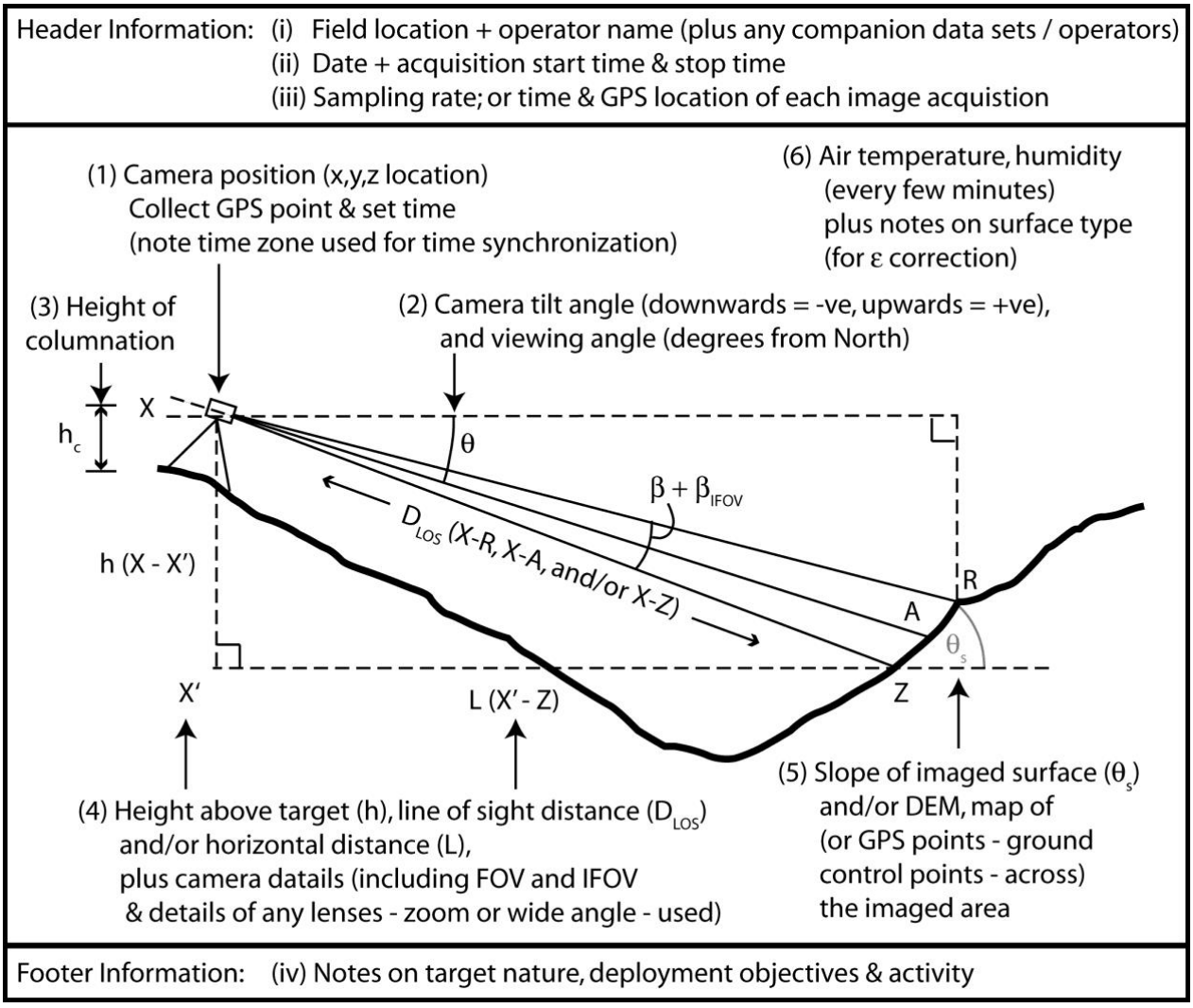

Figure 10: Parameters to be recorded in a field note book at the time of image acquisition to allow adequate geometric and atmospheric correction of a thermal image. DEM: Digital Elevation Model, GPS: Global Positioning System, (I) FOV: (Instantaneous) Field of View, LOS: Line of sight. From [Harris, 2013].

2.2.5. A short note on temperature retrievals from satellite-based sensors.

See Chapter Monitoring Heat for more details.

Satellite-based sensors operating in the thermal infrared (typically 10–14 μm), as well as in the mid (typically 3.5–4.0 μm) and shortwave (around 2.5 μm) infrared, can provide temperature information. However, these are pixel-integrated temperatures meaning that the measurement is an integration of all surfaces emitting within the pixel, which is typically 30 to 4000 m in dimension. Mixture modelling can retrieve this surface structure, but are subject to the need to oversimplify a complex problem. That is, a continuum of temperatures between background (ambient) and eruptive (ca. 1000 °C) need to be described by a mixture model with, typically, two components (hot and cold). Such mixture models are also blighted by issues of saturation, where gain settings were not designed for measurements over high temperature surfaces. Instead, the maximum temperature that can be recorded in the thermal infrared is typically 60–120 °C, and in the shortwave around 250 °C. Thus, over active lavas, all pixels are saturated with the only information available being that the temperature is greater than the saturation. Worse, the point spread function and optical reflection can cause intense smearing in the imagery and halo effects. Thus, satellite-based sensors are not, currently, well suited for retrieval of absolute temperature, but can be used for mapping as previously shown (also see Chapter Monitoring Heat).

2.3. Lava surface velocity

Surface velocity can be obtained from a series of images (or video) collected in the field either using a camera from the ground or flown on an UAS using particle velocimetry. This consists of tracking a particle, or a set of particles, on scaled digital photos or thermal images acquired at a known frequency. Velocity is then calculated from the distance travelled by the particle and the time between two images. For this, pixel size must be well known and calculated according to distance from the target and IFOV following the trigonometric relations as described in the in section 2.2.4. In case of images or video footage acquired via UAS, a nadir view is ideal as obtained with a stationary hover (to avoid image smearing) and a FOV covering the whole channel including the stationary levée to anchor the velocity, with a few minutes of recording being ideal (James et al. 2020). Particle velocimetry software, such as PIVlab (Thielicke and Stamhuis 2014), can be used to analysis a few minutes of video. Surface velocity may then be exploited to derive velocity profile over the full width and depth of the channelized lava (see section 3), and integrated with depth to estimate IER and its local fluctuation (e.g., Bailey et al., 2006; Harris et al., 2007; 2019; Dietterich et al. 2021) .

2.4. Sampling

Collecting rock samples during an eruption has the main objective of providing time-series for the physio-chemical properties of the magma so as to provide insights into the eruption source and allow initialization of lava flow simulation models (Harris et al., 2017, 2019). Following the evolution of texture, chemical composition and petrology during an eruption has come to be known as petrological monitoring and involves collection and distribution of data as soon as samples have been received, prepared and analyzed (e.g., Pankhurst et al. 2022; Gansecki et al. 2019).

Effective petrological monitoring involves sampling volcanic deposits as soon as, and as often as, possible during an ongoing eruption because the emitted lava may be buried the next day by a new flow or fallout. The main problem with sampling an active lava flows is often, though, not an easy task, as with thermocouple measurements, the access to the lava flow. Lava channels and tubes are often inaccessible, and recently emplaced and hot lava usually needs to be crossed to access the flow. Due to the heat, appropriate protective clothing, shield and sampling instrument need to be selected (**Fig. 11**). Sampling the cooler lava flow front or lateral levées is often easier, although falling blocks need to be watched for.

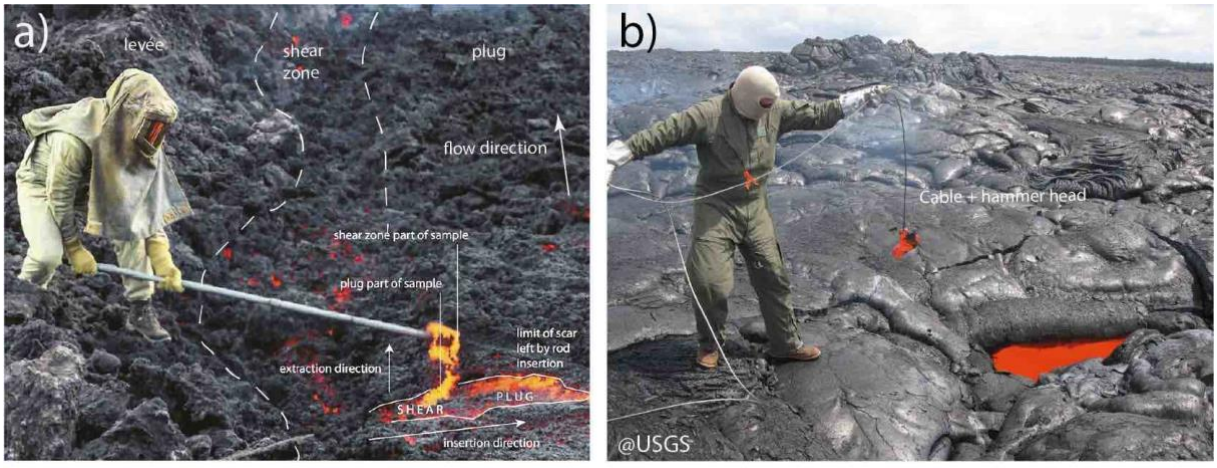

Figure 11: a) Sampling a lava channel from the stable levées (Piton de la Fournaise, La Réunion, 2015; (Harris et al. 2020); a heat suit and 2-m stainless steel pole welded to a scoop is used; all the same the boots of the operator began to flame just after this photograph was taken, sending toxic smoke up into the helmet. b) Sampling a lava tube through a skylight (Kilauea, Hawaii, 2010) (courtesy of USGS Hawaiian Volcano Observatory); here a hammer head on a cable is being used, and the operator has a fire-resistant balaclava and flight suit.

Samples of molten lava must be rapidly quenched in water, which will freeze-in the lava physico-chemical and textural properties before any modifications due to a slower cooling

(micro-crystallization, element diffusivity, post-sampling vesiculation and expansion). Such a sampling method ensures retrieval of the proportion of phases, glass composition and redox state (**Fig. 12**). But requires the following to be carried to the sampling site:

1. A sampling instruments (hammer, chain, shovel …);
2. Several liters of water for quenching;
3. A container to quench the sample in.

All of this is added equipment volume and weight to carry to the sampling site. Waiting for the sample to cool in air will result in complete crystallization of the groundmass as well as re-organization of the vesicle population. The resulting interstitial melt phase will therefore not be glassy and representative of the flow state, but instead will display a microcrystalline groundmass typical of slow, in-situ (post-emplacement) cooling (**Fig. 12**). This means that the microlite and bubble contents present during flow will be overprinted and lost. If the surface layer is naturally quenched so as to preserve a thin glassy rind, then this layer can be representative of the molten lava (**Fig. 12b**). However, such layers are hard to find, and the sample must be 'in-place'; meaning it is not a rafted fragment that was quenched closer to the vent and then transported down flow.

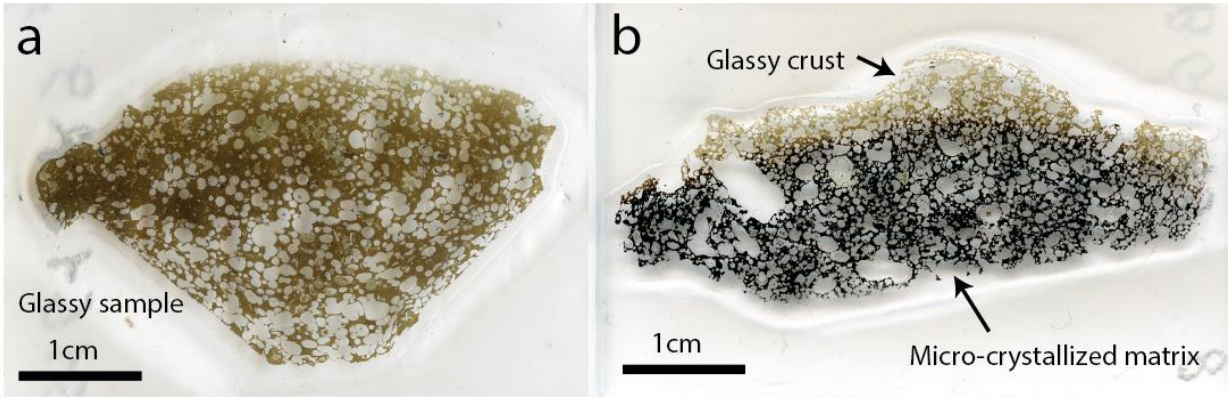

Figure 12: Polished thin sections (30 µm) of basaltic lava collected at Kilauea (Hawaii) in 2016. a) Lava sampled with a stainless-steel tool and quenched in water. The sample is entirely glassy and preserved crystal and bubble size distribution. b) Sample collected on a naturally cooled pāhoehoe lobe showing a glassy crust (brown color) and a non-glassy micro-crystallized interior (black color).

2.5. Lava flow morphology / typology

Lava flow type and associated morphology should be reported as it gives indication on the lava flow dynamics. The field book entries for the day include descriptions and sketches of:

1. The lava flow distribution system (channel, tube-fed, dispersed …);

2. Lava flow type (juvenile ‘ā’a, mature ‘ā’a, blocky, transitional, s-type / p-type pāhoehoe);
3. Flow field form (ridged, ogives, ramped, ropey, hummocky, sheet …);
4. Any associated features (skylights, lava balls, lava boats, tumuli, shatter rings …).

Included for each entry should be estimates of approximate dimensions, especially length, width, height and depth of any feature, as well as underlying and new surface slope (**Fig. 13**). Of course, titles, orientations, scales, dates, times, GNSS points and tags for photos taken should be entered.

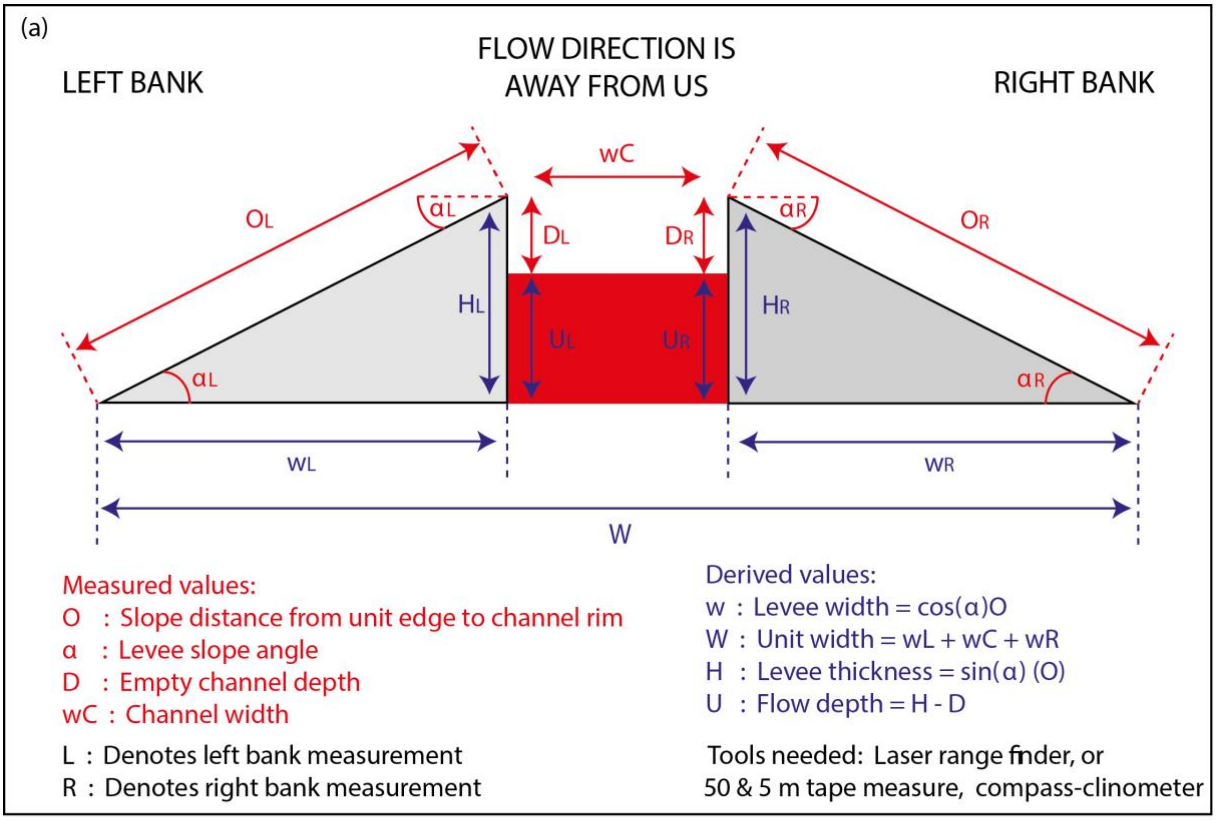

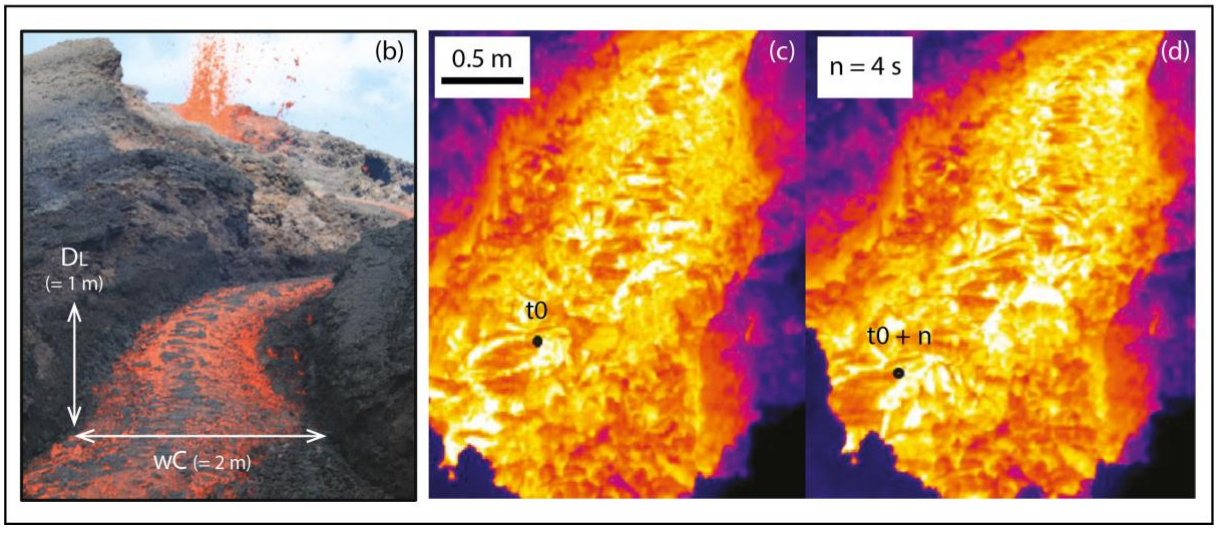

Figure 13: (a) Channel dimensions to be measured and calculated (modified from Harris et al., 2022), with (b) example of below bank flow from a channel active at Piton de La Fournaise (La Réunion) on 1 August 2015 (Harris et al., 2020). Dimensions were obtained from scaled digital photos and thermal images, with velocities also being obtained from the latter. Thermal images were collected at a frequency of 4 s. In (c) a piece of cooler crust has been selected as close to the channel center as possible, and found again in the next image obtained, as given in (d). The object has travelled 0.2 m in 4 s, so velocity is 0.05 m/s. Given the channel width and a square channel that is as wide as it is deep gives an effusion rate of $[2 \times 2 \times (0.67 \times 0.05 \text{ m/s})] = 0.13 \text{ m}^3/\text{s}$. Of course, the type of measurements and notes taken will depend on the feature under observation, where this case focuses on a vent-proximal lava channel.

3. First Order derivatives

3.1. Building DEMs and volume estimation

To assess future lava flow paths, the constantly changing topography needs to be updated. Commonly, DEMs are constructed by stereophotogrammetry that consists of merging georeferenced images taken from different angles. Images are either acquired by UAS (James et al., 2020), during flight surveys (Derrien 2019) or from satellite sensors operating in the visible (Bagnardi et al., 2016). To build a DEM either multiple ground control points (GCPs) are used to allow scaling and georeferencing (the larger the study area, the more GCPs are required) or, as usually done during an eruption, the images are geotagged which allows a decent georeferencing. Indeed, during an eruption establishing ground markers on foot is often impossible. Data processing then involves applying SfM technique using software such as Pix4D, Metashape or MicMac. Space agency services also produce DEMs from optical data (e.g., ASTER GDEM), from multi-view optical systems of high spatial resolution (e.g., tri-stereo Pleiades), or from radar data (e.g., SRTM and tanDEM-X; Zink et al. 2014).

LiDAR technique involves a pulsed laser that returns three-dimensional information of the pointed surface. After filtering, the obtained point cloud generates topography of bare earth and can be used in geographic information systems. LiDAR may either be mounted on an airplane or on an UAS and provide very high-spatial resolution DEMs (of a few cm), although at high cost (Cashman et al. 2013).

Reconstruction of new topography has two main goals. First, if topography is obtained rapidly and regularly it can be used to update and improve numerical simulations of lava flow paths. Second, the new DEM can be used to quantify the lava flow field volume. This is achieved by calculating the difference between the topography in the new DEM and that of the pre-existing DEM. Alternatively, first estimation of the lava volume can be calculated from the average thickness of the flow and the flow area. Thickness can either be measured on the field from flow edge height, from shadow in visible imagery if sun geometry can be calculated or from DEM. For long lasting eruptions, regular volume estimation and DEM acquisition is part of the

monitoring routine as it serves to produce volume time series. This can then be compared with volumes calculated by integrating TADR obtained via satellite over the period of time in between two images to check on the effects of data loss due to cloud cover in the latter data set.

3.2. Velocity profile and spreading rate

In the field, as well as in thermal and visible video, flow velocities can be obtained by timing the transit time of a marker, such as a piece of crust or the flow front, over a known distance (section 2.2.4).

3.2.1. Velocity profile

For surface measurements, the velocity will increase from a minimum velocity at the channel margins to a maximum (v_{max}) towards the center. The reverse will reply with depth where the velocity will decrease from a maximum at the surface to a minimum at the flow base (**Fig. 14**). It is thus important to place the measurement in terms of where it is taken within this velocity profile, where the safest approach is to take the maximum value at the channel center.

Considering a simple wide channel geometry and that lava rheological behavior is Newtonian, the calculated velocity profile can then be used, through the Jeffreys' (1925) equation, to set this measurement in spatial context. For a channel of width or depth *h*, velocity as a function of distance from the bank or base (z) can be calculated from:

$$v(z) = \frac{\rho g \sin(\alpha)(h^2 - z^2)}{4\eta} \quad (9)$$

Here, ρ is density, g is gravity, α is slope and η is viscosity, and the coordinate system is:

z = 0 at the channel center and/or surface (where $v(z) = v_{max}$), and

z = t at the channel margins and/or base (where $v(z) = 0$).

Other measurements taken at different points on the profile can be compared with the derived profile, and if the fit is good the average velocity (v_{mean}) can be obtained. The average is typically 0.67 × v_{max} (**Fig. 14a**) and can be calculated from,

$$v_{mean} = \frac{\rho g \sin(\alpha) h^2}{8\eta} \quad (10)$$

Thus, an important measurement to help constrain the velocity system is flow width and, if possible, depth where the equations can also be used to constrain flow velocities in now inactive channels or tubes. Another important piece of information is whether there is a plug, or zone of non-shearing lava, at the channel center. Across this plug all flow is at the same velocity, so that the velocity profile needs be calculated with the limits

z = 0 at the plug edge and/or base (where $v(z) = v_{max}$), and

z = t at the channel margins and/or base (where $v(z) = 0$),

as done in (**Fig. 14c**). The mean velocity can also be re-calculated to take into account that a yield strength needs to be overcome to flow so we are dealing with a Bingham, rather than Newtonian, fluid using (Moore 1987):

$$v_{mean} = \left(\frac{\rho g \sin(\alpha) h^2}{8\eta}\right)\left(1 - \frac{4}{3}\frac{\tau_0}{\tau} + \frac{1}{3}\left(\frac{\tau_0}{\tau}\right)^4\right) \quad (11)$$

Here, τ_0 is the yield strength, which can be calculated from plug width (w_p), where $\tau_0 = w_p \rho g \sin(\alpha)$, and τ is the basal shear stress [$\tau = \rho g h \sin(\alpha)$]. Thus, width of the plug is a final measurement that needs to be made.

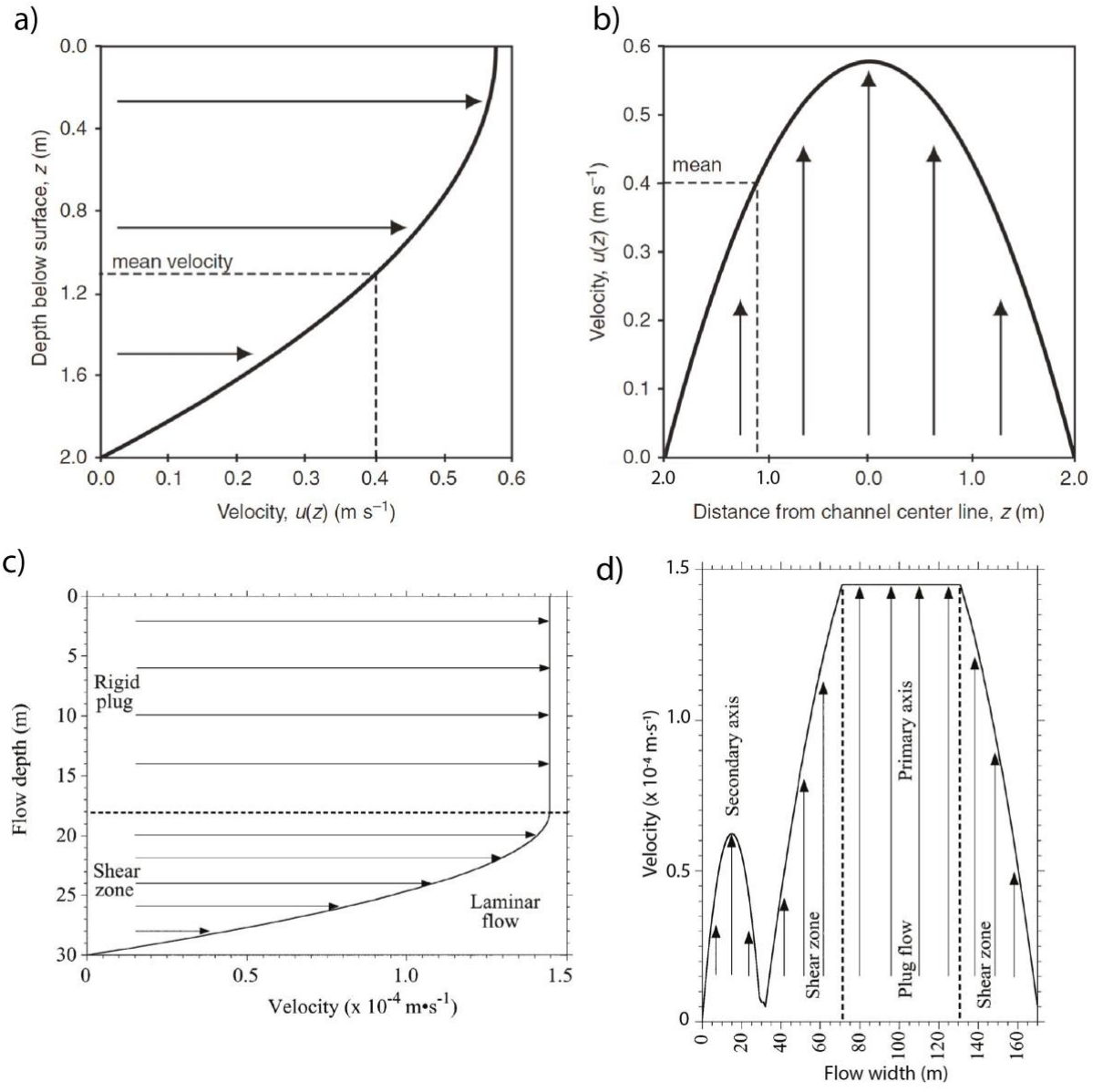

Figure 14: Vertical (a) and horizontal (b) velocity profiles for Newtonian flow (Etna, Italy, 2001, modified from Bailey et al., 2006), and for Bingham flow (c and d) (Santiaguito, Guatemala, 2001, modified from Harris et al., 2002)

650

651 ### 3.2.2. Spreading rate

652 If pixel dimension is known, feature width, length, perimeter and area (A) can be measured
653 from airborne thermal imagery. Changes from overflight to overflight can then be used to derive
654 advance velocities and spreading rates. Application of thermal chronometry can also be used to
655 estimate the time since emplacement (t). This is based on the characteristic cooling that the flow
656 surface experiences and which can be empirically described by (Hon et al. 1994):

657 $$T_{surf} = -140 \log(t) + 303 \quad (12)$$

658 Where t is time since emplacement in hours. Now the surface temperature can be used to
659 derived age from:

660 $$t = 146 \exp(-0.0164\ T_{surf}) \quad (13)$$

661 Lava area emplaced over given periods can now be mapped, and the area (ΔA) and time (Δt)
662 differential used to obtain spreading rate ($\Delta A/\Delta t$) (**Fig. 15**).

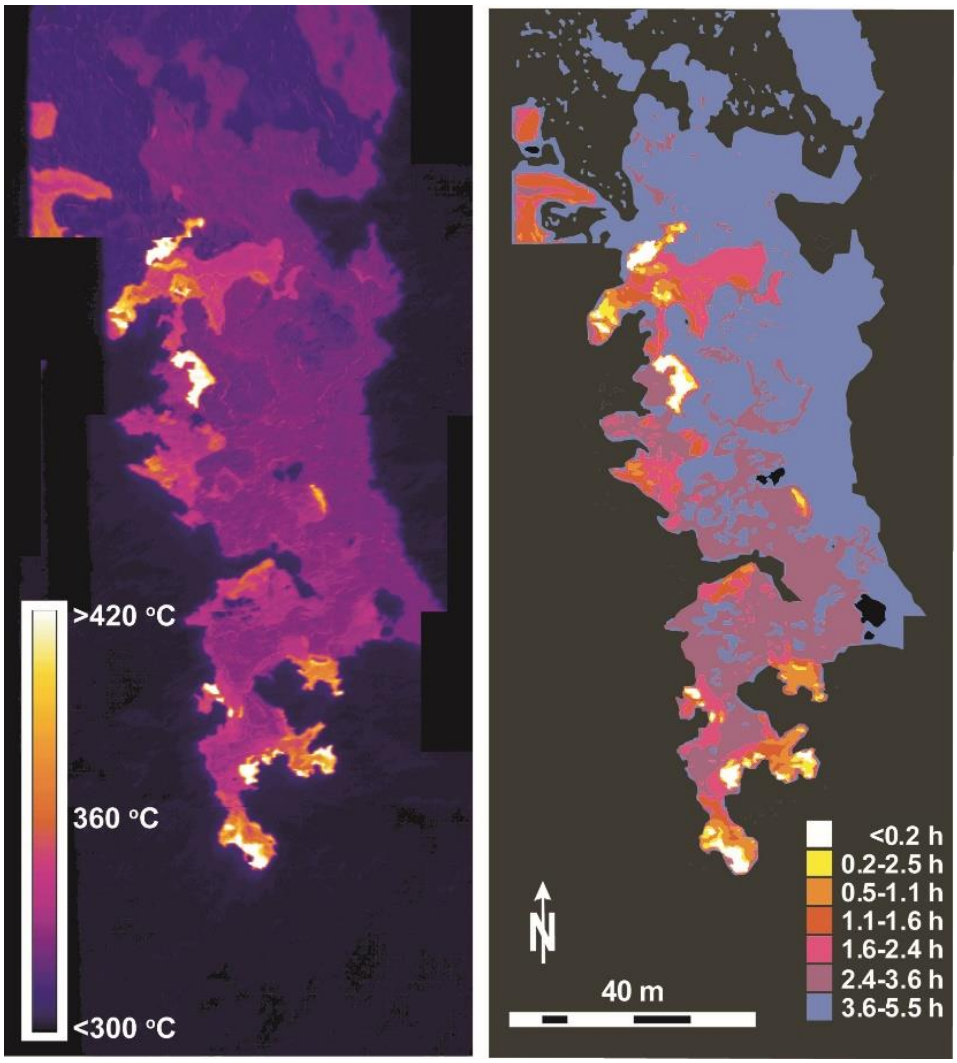

663 **Figure 15:** Surface temperature and conversion to time since emplacement for a pāhoehoe flow active on Kilauea
664 (Hawaii) in 2006. This is a mosaic of five images acquired vertically from a helicopter hovering 200 m above the

surface. An area of 2400 m² was covered in the 1.1 hour prior to acquisition to give a spreading rate of 2181 m² per hour. From (Harris et al., 2007).

3.3. Heat Loss and Cooling rate

The two main heat losses from a lava flow surface are due to radiation (Q_{rad}) and convection (Q_{conv}). In terms of heat flux density (W m^{-2}) these can be written:

$$Q_{rad} = \varepsilon \sigma (T_{surf}^4 - T_{amb}^4) \quad (14a)$$

$$Q_{conv} = h_c (T_{surf} - T_{amb}) \quad (14a)$$

In which σ is the Stefan Boltzmann constant (5.67 × 10^{-8} W m^{-2} K^{-4}), T_{surf} is the ambient temperature (in Kelvin) and h_c is the convective heat transfer coefficient (35–50 W m^{-2} K^{-1}). If flow depth (t) and mean velocity (v_{mean}) have also been measured, we can also estimate heat (in W m^{-2}) supplied from advection (Q_{adv}) and generated by crystallization (Q_{cryst}) from:

$$Q_{adv} = v_{mean}\, t\, \rho\, c_p\, (dT/dx) \quad (15a)$$

$$Q_{cryst} = v_{mean}\, t\, \rho\, C_L\, (d\phi/dT)\, (dT/dx) \quad (15b)$$

Here, c_p is lava specific heat capacity, dT/dx is the cooling rate per unit distance, C_L is latent heat of crystallization and dϕ/dT is fraction crystallized per degree cooling. This can be solved if dϕ/dT and/or dT/dx have been measured through sampling and/or thermocouple measurements at different down flow points. On the other hand, if dϕ/dT can be assumed, then cooling rate can be estimated.

We have a system whereby heat is supplied by Q_{adv} and Q_{cryst}, and lost by Q_{rad} and Q_{conv}. In our case, the heat lost is not balanced by heat supplied, i.e.,

$$Q_{rad} + Q_{conv} > Q_{adv} + Q_{cryst} \quad (16a)$$

As a result, the system is in disequilibrium and cools as a response. Given this imbalance, if we write the condition of 16a out in full and rearrange to isolate cooling, we arrive at:

$$\frac{dT}{dx} = \frac{Q_{rad}+Q_{conv}}{v_{mean} t \rho \left(c_p + c_L \frac{d\varphi}{dT}\right)} \quad (16b)$$

This approximation can be used to estimate potential flow length (e.g. Harris and Rowland, 2001). For example, if the cooling rate is 10 °C per kilometer, and the difference between eruption temperature and solidus or the point at which the flow can no longer move is 300 °C, then the maximum likely cooling-limited run out is 30 km. This back of the envelop calculation is very much an approximation, but can give a first order idea as to likely flow run out.

3.4. Sample chemical composition and texture

Analyzing rocks take time because samples need to be cut, powdered and polished thin sections produced. For a long time, sample analyses were therefore only used for scientific research purposes. However, in the last decades, analytical analyses have become faster and more sophisticated petrological monitoring has now becoming more efficient (Re et al. 2021). Early petrological monitoring of effusive activity at Kilauea by HVO during the 1980s and 1990s contributed to assessing the state of the magmatic system feeding effusion (e.g. Thornber et al., 2003). Analyzes also allowed tracking of eruption temperatures and cooling rates through application of glass geothermometry (Helz et al. 2003).

More recently, the response system such as DYNVOLC (operated by OPGC, http://dx.doi.org/10.25519/DYNVOLC-Database) allows providing petrological and textural analyses during any and all eruptions of Piton de la Fournaise (La Réunion) within a few days of sample collection to contribute to monitoring efforts by the observatory (Harris et al., 2017). This response system was also applied recently during the submarine eruption offshore of Mayotte where Berthod et al. (2021) performed detailed petrographic analyses of collected submarine samples to contribute to monitoring efforts. Another recent example is Pankhurst et al. (2022) who published a report on the rapid petrological monitoring response to the La Palma eruption with combined field, petrographic and geochemical analyses conducted within 10 days of sampling.

Petrological monitoring is therefore a key action to best constrain and understand an ongoing effusive event (Gansecki et al. 2019). The first information to obtain is bulk rock chemistry, including major and trace elements. Major element composition is essential to rock type classification and for physical properties to be determined such as density and viscosity, essential for lava flow modeling. Trace elements, although not used for lava flow modelling, inform on the magma storage conditions and ascent path, and evolution of these conditions through time. This is essential to track any changes of the magma properties and track whether there is a new magma recharge, or an evolution toward more silica-rich or volatile-rich composition that could force the eruption to transition toward explosive behavior.

Bulk chemistry is always accompanied with a detailed description of petrology and texture. Petrological analyses give information on the magmatic plumbing system including magma source depth, residence time, ascent rates, and ascent path. Magma reservoir depth (pressure) and temperature are essentially obtained through thermobarometry (see Putirka, (2008) for reviews). Crystal size distribution, crystal zonation, reaction rim features and presence of xenoliths are also used to constrain ascent rate and path. Textural analysis includes

consideration of density, porosity, percentage of crystals and vesicles, as well as, crystal and bubble size distributions (Guilbaud et al. 2007; Rust and Cashman 2011; Gurioli et al. 2008; Harris et al. 2020; Robert et al. 2014; Chevrel et al. 2018). These inform also on the ascent dynamics, especially for explosive phases because the texture is preserved at magma fragmentation. In the case of monitoring lava flows, sample analysis provides information on the lava temperature using geothermometry, cooling rate, crystallization history, phase (melt, crystal, bubble) proportion, redox state and, hence, thermo-rheological properties. Care should be taken when analyzing a sample given the sampling strategy (see section about sampling).

In essence, when monitoring a lava flow, it is essential to:

1. measure the bulk rock major element composition and volatile content,
2. estimate the temperature at the eruptive vent and then down flow to constrain cooling rate,
3. measure density including dense rock equivalent and derive porosity,
4. estimate the vesicle content and size distribution, and
5. estimate the crystal (phenocrysts and microlite) content and size distribution.

To constrain cooling and crystallization rate down flow, one must look for the phases that crystallized once the lava had been erupted, and not before, i.e., we need to use the microlites. Usually the phenocryst content does not change down a lava flow, but the microlite content often increases as the lava cools (Cashman et al. 1999).

4. Second order derivatives

4.1. Volumetric discharge rate (volume flux)

4.1.1. Instantaneous effusion rate from lava velocity

The effusion rate (E_r) of lava is given in m^3/s and defined as:

$$E_r = v\, d\, w \tag{17}$$

In which v, d and w are flow velocity, depth and width, respectively. The "simplest" way to calculate this is by measuring v, d and w in the field at an active channel or via a view of an active stream in a tube through a skylight. If measured at a point location over a short time this will provides the IER (see section 1.3.2).

Velocity can be estimated using the time needed for a surface marker, such as a distinctive piece of crust, to move across a known distance (section 2.2.4). Because velocity will vary across the channel (see **Fig. 14**), care must be taken to make this measurement at the channel center where velocity will be at a maximum. This can then be converted into an average

velocity, which for a parabolic flow profile will be v_{mean}=0.67v_{max}, taking care to correct for the presence of any plug. The average velocity needs to be used in Equation (17). Alternatively, velocity can be obtained from sequences of scaled digital photographs or thermal images (section 2.2.4; **Fig. 13c,d**). The same scaled images can be used to estimate channel width. Width can also be obtained using a laser range finder, although these are often very unreliable for low reflectance values, as is the case for basalt, as well as in heat haze or gassy conditions. Radar guns have also been used for flow in tubes.

Channel depth is more difficult to estimate, but may be approximated from levee or flow front height, taking into account a basal layer of crust and the level of flow below bank (**Fig. 13**). Alternatively, a channel shape (square, rectangular, or semicircular) can be assumed, and the width used to approximate depth for the given shape. Another option is to wait for the activity to stop, and directly measure the channel geometry directly with tape measure (**Fig. 10**), and then use this to estimate an average velocity using Equation (10). Attempts have been made by plunging iron bars into the flow, but this is remarkably difficult to do due to difficulty of access down into the channel for below bank flow, instability of levees, presence of impenetrable surface crusts, and extreme high temperature conditions. Attempts have been made to throw javelins into channel flow, but to no avail (Lipman and Banks 1987).

4.1.2. TADR from volume, heat budget and flow area

Volume flux can also be estimated by subtracting sequential volumes of the flow field and dividing by the time between each volume estimate, which give a TADR. Volume estimates are either obtained from geometry of the flow estimated and DEM subtraction (see section 3.1), or via satellite-based hot spot detection systems (see Monitoring heat chapter and (Coppola et al. 2010)) or via petrological method (Verdurme et al. 2022).

Another method to estimate TADR that has been well-used for satellite sensor-derived data in the thermal infrared, such as AVHRR and MODIS, is the heat budget approach (See Chapter Heat Monitoring). This assumes a direct relation between heat flux and TADR where heat flux increases linearly with TADR, i.e.,

$$TADR = x\,A\,(Q_{rad} + Q_{conv}) \quad (18)$$

where A is the flow area and x is a scaling factor that depends on local conditions such as slope, degree of insulation and rheology. The basis of this relation is that the greater the TADR, the greater the potential for the lava to spread (under any given slope, insulation and rheological condition) and so attain a greater area. Hence, TADR scales with $A \times (Q_{rad} + Q_{conv})$. Means of

scaling this relationship are reviewed in Harris (2013). A simpler approach is to assume that flow area increases with TADR, so that

$$TADR = x\,A \quad (19)$$

In both cases (18 and 19) the solution becomes an empirical one which can be solved using historical data for TADR and *A*, or theoretically (See Chapter Heat Monitoring).

4.1.3. Conversion to length

In a hazard sense, the most useful way to use effusion rate or TADR is to quickly assess how far a lava may extend at a given supply rate. This follows on from Walker (1973) who showed that lava flow length (*L*) tends to scale with TADR, so that

$$TADR = x\,L \quad (20)$$

As with the relations of (18) and (19), this scaling needs to be carried as a function of flow composition, rheology, slope and insulation. Again, this can be done using field data for TADR and *L* or theoretically, if all flow characteristics (type, cooling rate, petrology and rheology) and topography are approximately the same for all cases.

4.2. Rheological properties

Defining the rheological behavior of lava flows can be considered from two angles. The first is the lava material itself that depends on its chemical and petrographically characteristics. The second from the flow as viewed as a whole, considering the flow's dimension, velocity and morphology.

4.2.1. Rheology from lava sample characteristics

Defining the lava rheology from sample characteristics must be performed on samples collected along the flow, either collected after emplacement or from in situ sampling. Lavas are made up of three phases. The molten phase, the solid phase (the crystals) and the gas phase (bubbles). Most lavas are defined as suspensions, meaning that their crystal cargo is less than the random maximum crystal packing. Although multiple models exist to constrain the viscosity of a magmatic suspension (see review by Kolzenburg et al. 2022), a simple protocol can be applied to define it. In this case, the viscosity of a lava is set as the apparent viscosity (η_{app}) of a mixture of polydisperse particles (crystals and bubbles of various shapes and sizes) in a liquid phase (that is a silicate melt):

$$\eta_{app} = \eta_{melt} \cdot \eta_r = \eta_{melt}(T, X) \cdot \eta_{rc}(\phi c, r, \dot{\gamma}) \cdot \eta_{rb}(\phi b, Ca) \quad (21)$$

where the viscosity of the melt phase (η_{melt}) is Newtonian and depends on temperature (T) and composition (X). The relative viscosity due to the presence of a crystalline phase (η_{rc}) depends on the volumetric abundance of crystals (ϕc) and their aspect ratio (r), as well as the strain rate ($\dot{\gamma}$). The relative viscosity due to the presence of bubbles (η_{rb}) depends on the volumetric abundance of bubbles (ϕb) and their capillarity number (Ca), which depends on the melt viscosity, bubble surface tension and strain rate.

The melt phase viscosity can be estimated from its composition and temperature using an appropriate model or directly by measuring the temperature-viscosity relationship (Russell, et al 2022). This is straightforward to obtain for lava samples where the glass phase has been well preserved (*in situ* sampling and quenching or naturally quenched crust, **Fig. 12**) because the chemical composition (major elements) can be easily measured using a microprobe and temperature can be calculated from crystal-liquid geothermometer (Putirka 2008). In turn, if the glass has not been preserved, but instead there is a microcrystalline groundmass, an alternative method is to calculate the bulk groundmass composition obtained by subtracting the crystal chemical composition using the average mass density of the crystals to the bulk chemical composition (Ramírez-Uribe et al. 2021).

To estimate the effect of crystals and bubbles a detailed textural analysis is necessary. This must include quantification of the particle sizes, shapes (aspect ratio) and abundances (volume fraction). These characteristics are usually obtained from image analyses of thin sections and microphotographs (obtained from microscope or electronic microscope, backscattered electron images) and using software such as ImageJ (see for example Chevrel et al., 2018). There are a large number of models to calculate the effect of crystals and bubbles on lava viscosity considering either two phases (melt + crystals or bubbles) or three phases (melt + crystals + bubbles). All details of the models found in the literature for magmatic suspensions are presented in the review of Kolzenburg et al. 2022).

4.2.2. Rheology of a lava flow

The apparent rheological characteristics of a lava flow may be obtained from its dimension, velocity and morphology. During an eruption, the viscosity of the flowing lava is estimated from using either the velocities of lava flowing within channels or at flow fronts (e.g. (Harris et al. 2004; deGraffenried et al. 2021; Harris et al. 2020). Under the simplification that lava flows in a laminar fashion with no inflation following a Newtonian or Bingham behavior, modification of the Jeffreys' (1925) equation and derivative equations (e.g., Eq. 9, 10, 11) can

be rearranged to estimate viscosity (Nichols 1939). Apparent lava flow yield strength can also be obtained from its geometric parameters (Hulme, 1974).

A third alternative method to monitor the rheological properties of lava as it flows are direct *in situ* viscosity measurement (see Chevrel et al. (2019) for review). However, this method is still far from being possible as an operational tool as there is currently ongoing research on reliable instrument that could be deployed easily in the field to perform such measurement (Chevrel et al. 2023). In over 60 years (1948 to 2019), only eleven studies on field lava rheology measurements have been published. Research is still ongoing and it would perhaps in the future lead to a routine measurement.

5. Hazard product: Lava flow modelling

Monitoring lava flows is often accompanied by forecasting most probable flow paths and areas of flooding. The simplest way of forecasting lava flow path is to define the line of steepest descent (Kauahikaua 2007). In Hawaii, the lines of steepest descent lines have been defined for use as a general guide in forecasting the initial lava flow path in future eruptions and to assist emergency managers (Kauahikaua et al. 2017; Rowland et al. 2005). Long-term hazard maps are a way of visualizing areas that will most likely be impacted (Chevrel et al. 2021; Favalli et al. 2012; Del Negro et al. 2013). However, when an eruption starts, a short-term hazard map is more appropriate because it focuses on the location of the ongoing eruption and represents a given scenario for that is restricted to the downhill area from the vent or the fissure and the zone at risk. These numerical models have been developed to include satellite-derived source terms (mostly TADR) and to allow real-time lava flow emplacement simulations and projections [Wright et al. 2008; Ganci et al. 2012; Harris et al. 2019]. This is routinely produced at highly eruptive center like at Hawaii (Neal et al. 2019), Mt Etna in Italy (Vicari et al. 2011) and Piton de la Fournaise, La Réunion (see below). Such maps are good communication tools between scientists and stakeholders. Nonetheless to ensure a common understanding and to help in building effective mitigation strategies they need to be designed based on the needs of the end users (Chevrel et al. 2022). For this, engagement with end users (local authorities) is absolutely necessary.

Lava flow forecasts usually involve provision of model-derived the

1. area that will potentially be covered
2. most likely path and
3. distances the flow could reach.

Output depends on topography, slope, volume flux at the vent, total volume of lava emitted and/or the thermo-rheological properties of the lava. There are a number of numerical models that can be used to build short-term hazard maps but they all need to be pre-initialized, calibrated and validated (Harris et al. 2019; Vicari et al. 2011; Hyman et al. 2022). Pre-initialization and calibration rely on collection of source term data collected, and validation involves retrospective analyses on previous eruptions to best fit the model to reality.

Exemple at Piton de la Fournaise (La Réunion)

At Piton de la Fournaise (Le Réunion), since 2014 lava flow inundation areas have been forecast and modeled through a satellite-data driven protocol (Chevrel et al. 2022; Harris et al. 2017; 2019). This protocol determines the flow probable inundation area and runout distances via the DOWNFLOWGO numerical code that is a combination of DOWNFLOW, that provides the path of steepest descent and probable lava flow inundation area (Favalli et al. 2005), and FLOWGO that calculates the maximum cooling-limited runout of lava for a given effusion rate (Harris and Rowland, 2001). To operate this protocol on an operational basis and routinely during each eruption, a retrospective analysis of the April 2018 eruption was carried out (Harris et al., 2019). As part of the protocol, an initial hazard map is shared within the first hours of any eruption and, when needed, the map is updated as eruption conditions evolve (new vents opening, extension of tubes, change in TADR) (**Fig. 16**). The maps provide a fundamental communication tool between scientists and the authorities and have been developed through iterative dialog with local civil protection. Figure 16 shows the delivered products during the operational forecasting and monitoring response at Piton de la Fournaise for the December 2020 eruption. This includes a map of the eruption site where the line of steepest descent and the probable lava flow paths is shown together with the location of the eruptive vent and of the flow front. This short-term hazard map can be better constrained and updated through the eruption as TADR is known (**Fig 16b, c**) and lava flow outline is obtained either from satellite imagery or airborne photogrammetry (**Fig 16d)**.

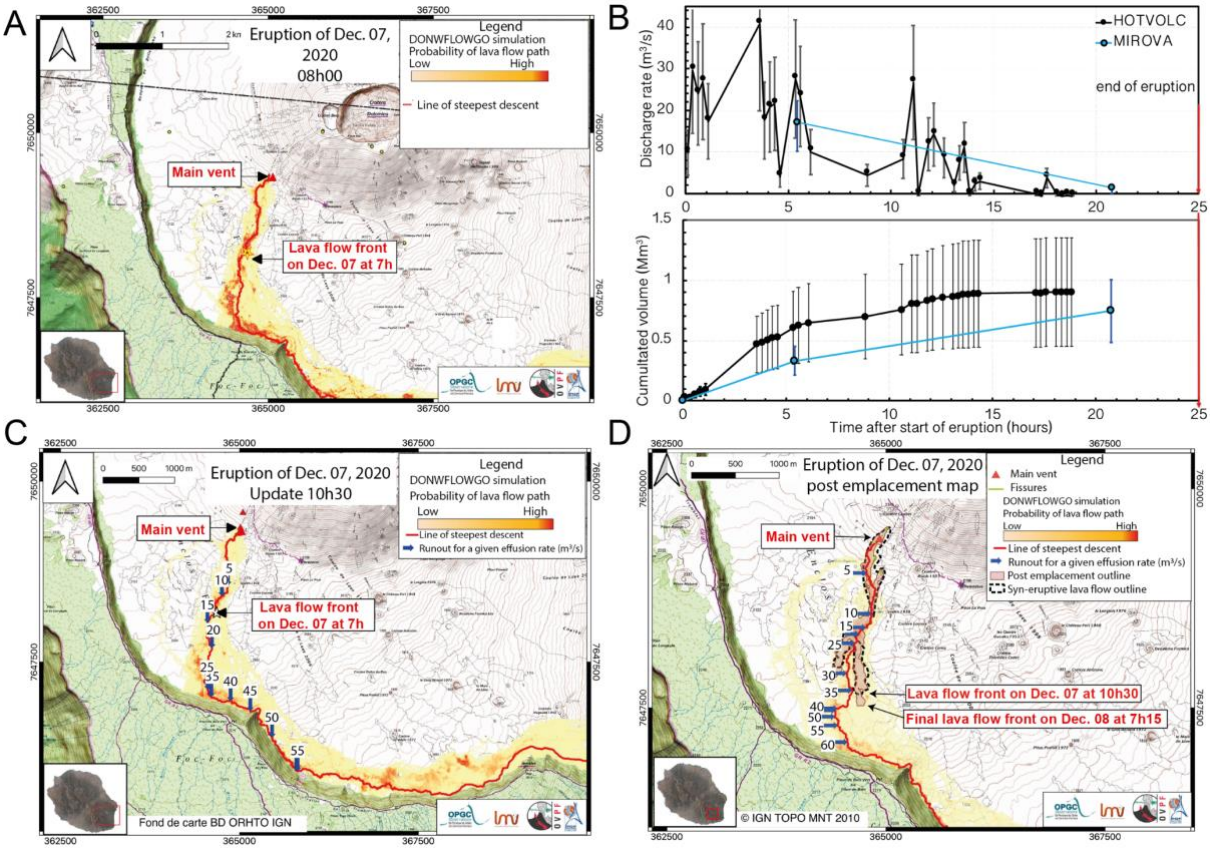

Figure 16: Operational forecasting and monitoring response at Piton de la Fournaise (La Réunion) for the December 2020 eruption. a) First map produced on December 7, 2020 at 8h00 local time. b) TADR and cumulative volume since the start of the eruption obtained by the HOTVOLC (Gouhier et al. 2016) and MIROVA (Coppola et al. 2016) systems. c) Updated map produced on December 7, 2020 at 10h30 local time. d) Final map showing the probability of lava flow invasion, runout distances as function of TADR and the final lava flow field outline obtained by airborne photogrammetry (post emplacement outline). The lava flow outline drawn from the Sentinel-2 image acquired on December 7 at 10h30 is also shown (syn-eruptive outline). This map was produced after the end of the eruption. Taken from Chevrel et al. (2022).

6. Lava flow monitoring: The future

Technology and capabilities are constantly improving and evolving, as new techniques come on line, existing instrumentation becomes improved, and prices become lower. One could argue that for monitoring, in some areas, we do not need any further reductions in images spatial resolution. For example, for lava flow modelling a DEM spatial resolution of 10 m is more than adequate. However, what we do need is the best possible temporal resolution, so as to track lava flow spreading, topographic trends and update lava flow models with the most up-to-date topography. Given the time scales involved in emplacement of a rapidly extending lava flow a few minutes may be ideal, whereas for longer lasting events (years) a few weeks may be sufficient. The key is, to balance data loads with scenario, processing capabilities and need. In populated areas the need for regular and fast processing of data and product, as developed by Copernicus Emergency Management Service (e.g., **Fig. 4**), is more pressing than in remote and unpopulated areas.

Of course, lava is hot so one of the best means of tracking it is remotely and in the infrared. However, no terrestrial sensor is currently perfect for tracking active lava. Fundamentally, gain settings are usually too low so that saturation occurs at 60–120 °C, meaning all pixels over an active lava flow are saturated. A pressing need is for at-least one waveband in the mid and/or thermal infrared with a saturation of at-least 800 °C.

UAS, that has literally taken off over the last decade, represent a promising tool to monitor lava flows but onboard thermal imaging payloads need to be developed for lava flow temperatures. To track entire lava flow fields, advances in UAS portable thermal imaging technology needs to be associated with improving capabilities for UAS to cover larger areas and for building orthomosaics from potentially thousands of images covering tens of km^2.

Seismicity and infrasound have been shown, especially during the 2018 eruption of Kilauea, capable of tracking the evolution of an effusive event, especially in terms of vent location and effusive intensity (Patrick et al. 2019). Further advances would be to track flow advance, where ground-based radar and/or InSAR could be used. This would be ideal for cloudy regions, but frequencies of current InSAR acquisitions could be increased to a few hours or so. Then, there are all sorts of possibilities we could think of, such as placing transmitting temperature and position sensors on and/or within an advancing lava flow.

While fast and simple non-physical 1 and 2D models are systematically used forecast lava flow paths and velocities and preparation of short term hazard maps (Harris et al. 2019; Chevrel et al. 2022; Ganci et al. 2012; Herault et al. 2009; Neal et al. 2019), more sophisticated physics-based models are still not well developed to produce a timely forecast (Dietterich et al. 2017). Development of faster numerical models accompanied by automatization of satellite data integration are needed so that such capabilities can be used as operational tools for efficient near real time lava flow propagation forecasting (Hyman et al. 2022; Cappello et al. 2022).

Automated reporting systems and observatory data bases are advancing all the time, so as to ease the administrative and reporting load of volcano observatory staff. Crowd sourcing through social media, will without a doubt, continue to develop as a resource to contribute to following effusive eruption impacts as well as distributing warning, alerts and information (Wadsworth et al. 2022). Conversely, there are other basics that are slow to improve: funding is never enough, staff numbers are always too low, helicopter time is frequently non-existent, and working hours are long, as are kilometers walked. The field practitioner will thus always argue in terms of reducing equipment weight and bulk along with a well-defined duty and task list, plus developing better means to keep drinking water cold and boots from burning.

7. References

Bailey, J E, A Harris, J Dehn, S Calvari, and S Rowland. 2006. "The Changing Morphology of an Open Lava Channel on Mt. Etna." *Bulletin of Volcanology* 68: 497–515.

Bato, M. G., J. L. Froger, A. J.L. Harris, and N. Villeneuve. 2016. "Monitoring an Effusive Eruption at Piton de La Fournaise Using Radar and Thermal Infrared Remote Sensing Data: Insights into the October 2010 Eruption and Its Lava Flows." *Geological Society Special Publication* 426 (1): 533–52. https://doi.org/10.1144/SP426.30.

Berthod, Carole, Etienne Médard, Patrick Bachèlery, Lucia Gurioli, Andrea Di Muro, Aline Peltier, Jean-Christophe Komorowski, et al. 2021. "The 2018-Ongoing Mayotte Submarine Eruption: Magma Migration Imaged by Petrological Monitoring." *Earth and Planetary Science Letters* 571: 117085. https://doi.org/https://doi.org/10.1016/j.epsl.2021.117085.

Biren, Jonas, Aneta Slodczyk, Joan Andújar, Leire del Campo, Lionel Cosson, Hao Li, Emmanuel Veron, Cécile Genevois, Sandra Ory, and Muhammad Aufaristama. 2022. "High Temperature Spectral Emissivity of Glass and Crystal-Bearing Basalts." *Journal of Volcanology and Geothermal Research*, 107623. https://doi.org/https://doi.org/10.1016/j.jvolgeores.2022.107623.

Blong, R J. 1984. *Volcanic Hazards, A Sourcebook on the Effects of Eruptions*. Edited by R J BLONG. *Volcanic Hazards*. Academic P. San Diego: Academic Press. https://doi.org/https://doi.org/10.1016/B978-0-12-107180-6.50010-X.

Burgi, Pierre Yves, Marc Caillet, and Steven Haefeli. 2002. "Field Temperature Measurements at Erta'Ale Lava Lake, Ethiopia." *Bulletin of Volcanology* 64 (7): 472–85. https://doi.org/10.1007/s00445-002-0224-3.

Calvari, S, M Cotteli, M Neri, M Pompilio, and V Scribano. 1994. "The 1991-1993 Etna Eruption: Chornology and Lava Flow-Field Evolution." *Acta Vulcanol.* 4: 1–14.

Cappello, Annalisa, Giuseppe Bilotta, and Gaetana Ganci. 2022. "Modeling of Geophysical Flows through GPUFLOW." *Applied Sciences (Switzerland)* 12 (9). https://doi.org/10.3390/app12094395.

Cashman, K. V., S. A. Soule, B. H. Mackey, N. I. Deligne, N. D. Deardorff, and H. R. Dietterich. 2013. "How Lava Flows: New Insights from Applications of Lidar Technologies to Lava Flow Studies." *Geosphere* 9 (6): 1664–80. https://doi.org/10.1130/GES00706.1.

Cashman, K V, C Thornber, and J P Kauahikaua. 1999. "Cooling and Crystallization of Lava in Open Channels, and the Transition of Pāhoehoe Lava to 'a'Ā." *Bulletin of*

Volcanology 61: 306–23. https://doi.org/https://doi.org/10.1007/s004450050299.

Chevrel, M.O., M Favalli, N Villeneuve, A J L Harris, A Fornaciai, N Richter, A Derrien, P Boissier, A Di Muro, and A Peltier. 2021. "Lava Flow Hazard Map of Piton de La Fournaise Volcano." *Natural Hazards and Earth System Sciences* 21 (8): 2355–77. https://doi.org/10.5194/nhess-21-2355-2021.

Chevrel, M.O., A J L Harris, M.R. James, L. Calabrò, L. Gurioli, and H. Pinkerton. 2018. "The Viscosity of Pāhoehoe Lava: In Situ Syn-Eruptive Measurements from Kilauea, Hawaii." *Earth and Planetary Science Letters* 493: 161–71. https://doi.org/10.1016/j.epsl.2018.04.028.

Chevrel, M.O., A J L Harris, A. Peltier, N. Villeneuve, D. Coppola, M. Gouhier, and S. Drenne. 2022. "Volcanic Crisis Management Supported by near Real Time Lava Flow Hazard Assessment at Piton de La Fournaise, La Réunion." *Volcanica* 5 (2): 313–34. https://doi.org/10.30909/vol.05.02.313334.

Chevrel, M.O., T. Latchimy, L. Batier, and R. Delpoux. 2023. "A New Portable Field Rotational Viscometer for High-Temperature Melts." *Reviews in Scientific Instrument* Submitted.

Chevrel, M.O., H. Pinkerton, and A.J.L. Harris. 2019. "Measuring the Viscosity of Lava in the Field: A Review." *Earth-Science Reviews* 196. https://doi.org/10.1016/j.earscirev.2019.04.024.

Copernicus Emergency Management Service. 2022. "Directorate Space, Security and Migration, European Commission Joint Research Centre (EC JRC)." Web. 12 July 2022. <https://emergency.copernicus.eu/>. https://emergency.copernicus.eu/.

Coppola, D., M. R. James, T. Staudacher, and C. Cigolini. 2010. "A Comparison of Field- and Satellite-Derived Thermal Flux at Piton de La Fournaise: Implications for the Calculation of Lava Discharge Rate." *Bulletin of Volcanology* 72 (3): 341–56. https://doi.org/10.1007/s00445-009-0320-8.

Coppola, D., M. Laiolo, C. Cigolini, D. Delle Donne, and M. Ripepe. 2016. "Enhanced Volcanic Hot-Spot Detection Using MODIS IR Data: Results from the MIROVA System." In *Detecting, Modelling and Responding to Effusive Eruptions*, edited by A.J.L. Harris, T. De Groeve, F. Garel, and S. A. Carn, 426:181–205. London: The Geological Society Special Publications. https://doi.org/10.1144/SP426.5.

deGraffenried, R., J. Hammer, H. Dietterich, R. Perroy, M. Patrick, and T. Shea. 2021. "Evaluating Lava Flow Propagation Models with a Case Study from the 2018 Eruption of Kīlauea Volcano, Hawai'i." *Bulletin of Volcanology* 83 (11).

https://doi.org/10.1007/s00445-021-01492-x.

Derrien, A. 2019. “Apports Des Techniques Photogrammétriques À l’étude Du Dynamisme Des Structures Volcaniques Du Piton de La Fournaise.” Université de Paris. http://www.theses.fr/2019UNIP7084.

Dietterich, Hannah R., Angela K. Diefenbach, S. Adam Soule, Michael H. Zoeller, Matthew P. Patrick, Jon J. Major, and Paul R. Lundgren. 2021. “Lava Effusion Rate Evolution and Erupted Volume during the 2018 Kīlauea Lower East Rift Zone Eruption.” *Bulletin of Volcanology* 83 (4). https://doi.org/10.1007/s00445-021-01443-6.

Dietterich, Hannah R., Einat Lev, Jiangzhi Chen, Jacob A. Richardson, and Katharine V. Cashman. 2017. “Benchmarking Computational Fluid Dynamics Models of Lava Flow Simulation for Hazard Assessment, Forecasting, and Risk Management.” *Journal of Applied Volcanology* 6 (1). https://doi.org/10.1186/s13617-017-0061-x.

Dietterich, Hannah R., Michael P. Poland, David A. Schmidt, Katharine V. Cashman, David R. Sherrod, and Arkin Tapia Espinosa. 2012. “Tracking Lava Flow Emplacement on the East Rift Zone of Klauea, Hawaii, with Synthetic Aperture Radar Coherence.” *Geochemistry, Geophysics, Geosystems* 13 (5): 1–17. https://doi.org/10.1029/2011GC004016.

Favalli, Massimiliano, Maria Teresa Pareschi, Augusto Neri, and Ilaria Isola. 2005. “Forecasting Lava Flow Paths by a Stochastic Approach.” *Geophysical Research Letters* 32 (3): 1–4. https://doi.org/10.1029/2004GL021718.

Favalli, Massimiliano, Simone Tarquini, Paolo Papale, Alessandro Fornaciai, and Enzo Boschi. 2012. “Lava Flow Hazard and Risk at Mt. Cameroon Volcano.” *Bulletin of Volcanology* 74 (2): 423–39. https://doi.org/10.1007/s00445-011-0540-6.

Ganci, Gaetana, Annamaria Vicari, Annalisa Cappello, and Ciro Del Negro. 2012. “An Emergent Strategy for Volcano Hazard Assessment: From Thermal Satellite Monitoring to Lava Flow Modeling.” *Remote Sensing of Environment* 119: 197–207. https://doi.org/10.1016/j.rse.2011.12.021.

Gansecki, Cheryl, R Lopaka Lee, Thomas Shea, Steven P Lundblad, Ken Hon, and Carolyn Parcheta. 2019. “The Tangled Tale of Kīlauea’s 2018 Eruption as Told by Geochemical Monitoring” 1212 (December). https://doi.org/10.1126/science.aaz0147.

Gouhier, M., Y. Guéhenneux, P. Labazuy, P. Cacault, J. Decriem, and S. Rivet. 2016. “HOTVOLC: A Web-Based Monitoring System for Volcanic Hot Spots.” In *Detecting, Modelling and Responding to Effusive Eruptions*, edited by A.J.L. Harris, T. De Groeve, F. Garel, and S. A. Carn, 426:223–41. London: The Geological Society Special

Publications. https://doi.org/10.1144/SP426.31.

Guilbaud, M. N., S. Blake, T. Thordarson, and S. Self. 2007. "Role of Syn-Eruptive Cooling and Degassing on Textures of Lavas from the Ad 1783-1784 Laki Eruption, South Iceland." *Journal of Petrology* 48 (7): 1265–94. https://doi.org/10.1093/petrology/egm017.

Gurioli, L., A J L Harris, B. F. Houghton, M. Polacci, and M. Ripepe. 2008. "Textural and Geophysical Characterization of Explosive Basaltic Activity at Villarrica Volcano." *Journal of Geophysical Research: Solid Earth* 113 (8): 1–16. https://doi.org/10.1029/2007JB005328.

Hansell, Anna, and Clive Oppenheimer. 2004. "Health Hazards from Volcanic Gases: A Systematic Literature Review." *Archives of Environmental Health* 59 (12): 628–39. https://doi.org/10.1080/00039890409602947.

Harris, A J L. 2013a. *Thermal Remote Sensing of Active Volcanoes: A User's Manual*. Cambridge: Cambridge University Press. https://doi.org/DOI: 10.1017/CBO9781139029346.

———. 2013b. *Thermal Remote Sensing of Active Volcanoes*. *Cambridge University Press*. Vol. 100. Cambridge: Cambridge University Press. https://doi.org/10.1017/CBO9781139029346.

———. 2015. "Basaltic Lava Flow Hazard." In *Volcanic Hazards, Risks, and Disasters.*, 17–46. https://doi.org/10.1016/B978-0-12-396453-3.00002-2.

Harris, A J L, M.O. Chevrel, D. Coppola, M S Ramsey, A. Hrysiewicz, S. Thivet, N. Villeneuve, et al. 2019. "Validation of an Integrated Satellite-data-driven Response to an Effusive Crisis: The April–May 2018 Eruption of Piton de La Fournaise." *Annals of Geophysics* 61. https://doi.org/10.4401/ag-7972.

Harris, A J L, J. Dehn, and S. Calvari. 2007. "Lava Effusion Rate Definition and Measurement: A Review." *Bulletin of Volcanology* 70 (1): 1–22. https://doi.org/10.1007/s00445-007-0120-y.

Harris, A J L, Jonathan Dehn, Mike R. James, Christopher Hamilton, Richard Herd, Luigi Lodato, and Andrea Steffke. 2007. "Pāhoehoe Flow Cooling, Discharge, and Coverage Rates from Thermal Image Chronometry." *Geophysical Research Letters* 34 (19): 1–6. https://doi.org/10.1029/2007GL030791.

Harris, A J L, L. P. Flynn, O. Matías, and W. I. Rose. 2002. "The Thermal Stealth Flows of Santiaguito Dome, Guatemala: Implications for the Cooling and Emplacement of Dacitic Block-Lava Flows." *Bulletin of the Geological Society of America* 114 (5): 533–46.

https://doi.org/10.1130/0016-7606(2002)114<0533:TTSFOS>2.0.CO;2.

Harris, A J L, Luke P Flynn, Otoniel Matias, William I Rose, and Julio Cornejo. 2004. "The Evolution of an Active Silicic Lava Flow Field : An ETM + Perspective" 135: 147–68. https://doi.org/10.1016/j.jvolgeores.2003.12.011.

Harris, A J L, S. Mannini, S. Thivet, M.O. Chevrel, L. Gurioli, N. Villeneuve, A.D. Muro, and A. Peltier. 2020. "How Shear Helps Lava to Flow." *Geology* 48 (2). https://doi.org/10.1130/G47110.1.

Harris, A J L, and S K Rowland. 2001. "FLOWGO: A Kinematic Thermo-Rheological Model for Lava Flowing in a Channel." *Bulletin of Volcanology* 63: 20–44. https://doi.org/10.1007/s004450000120.

Harris, A J L, Scott K Rowland, and Magdalena Oryaëlle Chevrel. 2022. *The Anatomy of a Channel - Fed ' a ' ā Lava Flow System*. *Bulletin of Volcanology*. Springer Berlin Heidelberg. https://doi.org/10.1007/s00445-022-01578-0.

Harris, A J L, N. Villeneuve, A. Di Muro, V. Ferrazzini, A. Peltier, D. Coppola, M. Favalli, et al. 2017. "Effusive Crises at Piton de La Fournaise 2014-2015: A Review of a Multi-National Response Model." *Journal of Applied Volcanology* 6 (1): 11. https://doi.org/10.1186/s13617-017-0062-9.

Helz, Rosalind, C Heliker, Ken Hon, and M Mangan. 2003. "Thermal Efficiency of Lava Tubes in the Pu'u 'Ō'ō-Kū Paianaha Eruption." *US Geological Survey Professional Paper*, 105–20.

Herault, A, G Bilotta, A Vicari, E Rustico, and C Del Negro. 2009. "Forecasting Lava Flow Hazards during the 2006 Etna Eruption: Using the MAGFLOW Cellular Automata Model." *Journal of Volcanology and Geothermal Research* 112 (1): 78–88. https://doi.org/10.1016/j.cageo.2007.10.008.

Hon, K, J P Kauahikaua, R Denlinger, and K Mackay. 1994. "Emplacement and Inflation of Pahoehoe Sheet Flows: Observations and Measurements of Active Lava Flows on Kilauea Volcano, Hawaii." *Geol. Soc. Am. Bull.* 106: 351–70.

Hulme, G. 1974. "The Interpretation of Lava Flow Morphology." *Geophys. J. R. Astron. Soc.* 39: 361–83.

Hyman, D M R, H R Dietterich, and M R Patrick. 2022. "Toward Next-Generation Lava Flow Forecasting: Development of a Fast, Physics-Based Lava Propagation Model." *Journal of Geophysical Research: Solid Earth* 127 (10): e2022JB024998. https://doi.org/https://doi.org/10.1029/2022JB024998.

James, Mike R., Brett B. Carr, Fiona D'Arcy, Angela K. Diefenbach, Hannah R. Dietterich,

Alessandro Fornaciai, Einat Lev, et al. 2020. “Volcanological Applications of Unoccupied Aircraft Systems (UAS): Developments, Strategies, and Future Challenges.” *Volcanica* 3 (1): 64–114. https://doi.org/10.30909/vol.03.01.67114.

Jeffreys, H. 1925. “The Flow of Water in an Inclined Channel of Rectangular Section.” *Philosophy Magasin* serie 6, 4: 293,793-807.

Kauahikaua, J P. 2007. “Lava Flow Hazard Assessment, as of August 2007, for Kilauea East Rift Zone Eruptions, Hawai`i Island.” *Open-File Report*. Version 1. https://doi.org/10.3133/ofr20071264.

Kauahikaua, J P, T. Orr, M R Patrick, and F. Trusdell. 2017. “Steepest-Descent Lines for Kīlauea, Mauna Loa, Hualālai, and Mauna Kea Volcanoes, Hawai‘i.” *U.S. Geological Survey Data Release*. https://doi.org/10.5066/F7FJ2DX0.

Keszthelyi, L. 1995. “A Preliminary Thermal Budget for Lava Tubes on the Earth and Planets.” *J. Geophys. Res.* 100: 20,411-20,420.

Kolzenburg, S., M.O. Chevrel, and D.B. Dingwell. 2022. “Magma Suspension Rheology.” *Reviews in Mineralogy and Geochemitry* 87 (1): 639–720. http://dx.doi.org/10.2138/rmg.2020.86.X.

Lipman, P W, and N G Banks. 1987. “Aa Flow Dynamics, 1984 Mauna Loa Eruption.” *U.S. Geol. Surv. Prof. Pap 1350*, 1527–67.

Meredith, Elinor S., Susanna F. Jenkins, Josh L. Hayes, Natalia Irma Deligne, David Lallemant, Matthew Patrick, and Christina Neal. 2022. “Damage Assessment for the 2018 Lower East Rift Zone Lava Flows of Kīlauea Volcano, Hawai‘i.” *Bulletin of Volcanology* 84 (7). https://doi.org/10.1007/s00445-022-01568-2.

Moore, H.J. 1987. “Preliminary Estimates of the Rheological Properties of 1984 Mauna Loa Lava.” *U.S. Geological Survey Professional Paper 1350* 99: 1569–88.

Neal, C A, S R Brantley, L Antolik, J L Babb, M Burgess, K Calles, M Cappos, et al. 2019. “The 2018 Rift Eruption and Summit Collapse of Kīlauea Volcano.” *Science* 363 (6425): 367–74. https://doi.org/10.1126/science.aav7046.

Negro, C. Del, A. Cappello, M. Neri, G. Bilotta, A. Herault, and G. Ganci. 2013. “Lava Flow Hazards at Mount Etna : Constraints Imposed by Eruptive History and Numerical Simulations.” *Scentific Reports* 3 (3493): 1–8. https://doi.org/10.1038/srep03493.

Nichols, R L. 1939. “Viscosity of Lava.” *The Journal of Geology* 47 (3): 290–302.

Oppenheimer, C. 1991. “Lava Flow Cooling Estimated from Landsat Thematic Mapper Infrared Data: The Lonquimay Eruption (Chile, 1989).” *Journal of Geophysical Research* 96 (B13). https://doi.org/10.1029/91jb01902.

Pallister, John, Rick Wessels, Julie Griswold, Wendy McCausland, Nugraha Kartadinata, Hendra Gunawan, Agus Budianto, and Sofyan Primulyana. 2019. "Monitoring, Forecasting Collapse Events, and Mapping Pyroclastic Deposits at Sinabung Volcano with Satellite Imagery." *Journal of Volcanology and Geothermal Research* 382: 149–63. https://doi.org/10.1016/j.jvolgeores.2018.05.012.

Pankhurst, Matthew J., Jane H. Scarrow, Olivia A. Barbee, James Hickey, Beverley C. Coldwell, Gavyn K. Rollinson, José A. Rodríguez-Losada, et al. 2022. "Rapid Response Petrology for the Opening Eruptive Phase of the 2021 Cumbre Vieja Eruption, La Palma, Canary Islands." *Volcanica* 5 (1): 1–10. https://doi.org/10.30909/vol.05.01.0110.

Patrick, M R, H. R. Dietterich, J. J. Lyons, A. K. Diefenbach, C. Parcheta, K. R. Anderson, A. Namiki, I. Sumita, B. Shiro, and J. P. Kauahikaua. 2019. "Cyclic Lava Effusion during the 2018 Eruption of Kīlauea Volcano." *Science* 366 (6470). https://doi.org/10.1126/science.aay9070.

Patrick, M R, Tim Orr, Gary Fisher, Frank Trusdell, and James Kauahikaua. 2017. "Thermal Mapping of a Pāhoehoe Lava Flow, Kīlauea Volcano." *Journal of Volcanology and Geothermal Research* 332: 71–87. https://doi.org/10.1016/j.jvolgeores.2016.12.007.

Poland, Michael P. 2022. "Synthetic Aperture Radar Volcanic Flow Maps (SAR VFMs): A Simple Method for Rapid Identification and Mapping of Volcanic Mass Flows." *Bulletin of Volcanology* 84 (3): 32. https://doi.org/10.1007/s00445-022-01539-7.

Putirka, K. 2008. "Thermometers and Barometers for Volcanic Systems." *Putirka, K., Tepley, F. (Eds.), Minerals, Inclusions and Volcanic Processes, Reviews in Mineralogy and Geochemistry, Mineralogical Soc. Am.* 69: 61–120.

Ramírez-Uribe, I., C. Siebe, M.O. Chevrel, and Christopher T. Fisher. 2021. "Rancho Seco Monogenetic Volcano (Michoacán, Mexico): Petrogenesis and Lava Flow Emplacement Based on LiDAR Images." *Journal of Volcanology and Geothermal Research* 411. https://doi.org/10.1016/j.jvolgeores.2020.107169.

Re, Giuseppe, Rosa Anna Corsaro, Claudia D'Oriano, and Massimo Pompilio. 2021. "Petrological Monitoring of Active Volcanoes: A Review of Existing Procedures to Achieve Best Practices and Operative Protocols during Eruptions." *Journal of Volcanology and Geothermal Research* 419: 107365. https://doi.org/10.1016/j.jvolgeores.2021.107365.

Robert, B, A Harris, G Gurioli, E Medard, A Sehlke, and A Whittington. 2014. "Textural and Rheological Evolution of Basalt Flowing down a Lava Channel." *Bulletin of Volcanology* 76: 824.

Rose, William I. 1987. “Volcanic Activity at Santiaguito Volcano, 1976-1984.” *Special Paper of the Geological Society of America* 212: 17–27. https://doi.org/10.1130/SPE212-p17.

Rowland, S K, H Garbeil, and A J L Harris. 2005. “Lengths and Hazards from Channel-Fed Lava Flows on Mauna Loa, Hawaii, Determined from Thermal and Downslope Modeling with FLOWGO.” *Bulletin of Volcanology* 67: 634–47. https://doi.org/https://doi.org/10.1007/s00445-004-0399-x.

Russell, James K, Kai-Uwe Hess, and Donald B Dingwell. 2022. “Models for Viscosity of Geological Melts.” *Reviews in Mineralogy and Geochemistry* 87 (1): 841–85. https://doi.org/10.2138/rmg.2022.87.18.

Rust, A. C., and K. V. Cashman. 2011. “Permeability Controls on Expansion and Size Distributions of Pyroclasts.” *Journal of Geophysical Research: Solid Earth* 116 (11): 1–17. https://doi.org/10.1029/2011JB008494.

Schmidt, Anja. 2015. “Volcanic Gas and Aerosol Hazards from a Future Laki-Type Eruption in Iceland.” In *Hazards and Disasters Series*, edited by John F Shroder and Paolo B T - Volcanic Hazards Papale Risks and Disasters, 377–97. Boston: Elsevier. https://doi.org/https://doi.org/10.1016/B978-0-12-396453-3.00015-0.

Thielicke, William, and Eize J. Stamhuis. 2014. “PIVlab – Towards User-Friendly, Affordable and Accurate Digital Particle Image Velocimetry in MATLAB.” *Journal of Open Research Software* 2. https://doi.org/10.5334/jors.bl.

Thornber, Carl R, Ken Hon, Christina Heliker, and David A Sherrod. 2003. “A Compilation of Whole-Rock and Glass Major-Element Geochemistry of Kïlauea Volcano, Hawaii, near-Vent Eruptive Products: January 1983 through September 2001.” *Open File Report 03-477*, no. January 1983: 8.

Verdurme, Pauline, Simon Carn, A J L Harris, Diego Coppola, Andrea Di Muro, Santiago Arellano, and Lucia Gurioli. 2022. “Lava Volume from Remote Sensing Data: Comparisons with Reverse Petrological Approaches for Two Types of Effusive Eruption.” *Remote Sensing* 14 (2). https://doi.org/10.3390/rs14020323.

Vicari, A., G. Bilotta, S. Bonfiglio, A. Cappello, G. Ganci, A. H??rault, E. Rustico, G. Gallo, and C. Del Negro. 2011. “Lav@hazard: A Web-Gis Interface for Volcanic Hazard Assessment.” *Annals of Geophysics* 54 (5): 662–70. https://doi.org/10.4401/ag-5347.

Wadsworth, Fabian B., Edward W. Llewellin, Jamie I. Farquharson, Janina K. Gillies, Ariane Loisel, Léon Frey, Evgenia Ilyinskaya, et al. 2022. “Crowd-Sourcing Observations of Volcanic Eruptions during the 2021 Fagradalsfjall and Cumbre Vieja Events.” *Nature Communications* 13 (1): 1–5. https://doi.org/10.1038/s41467-022-30333-4.

Walker, G P L. 1973. “Lengths of Lava Flows.” *Philosophical Transactions of the Royal Society, London* 274: 107–18.

Zink, Manfred, Markus Bachmann, Benjamin Brautigam, Thomas Fritz, Irena Hajnsek, Alberto Moreira, Birgit Wessel, and Gerhard Krieger. 2014. “TanDEM-X: The New Global DEM Takes Shape.” *IEEE Geoscience and Remote Sensing Magazine* 2 (2): 8–23. https://doi.org/10.1109/MGRS.2014.2318895.